Fall 2018

BLACK PHOSPHORUS QUANTUM DOTS: SYNTHESIS, CHARACTERIZATION, AND UTILIZATION TOWARDS THE PHOTOGENERATION OF HYDROGEN GAS

Charles Alfred Ayotte
University of New Hampshire, Durham

BLACK PHOSPHORUS QUANTUM DOTS: SYNTHESIS, CHARACTERIZATION, AND UTILIZATION TOWARDS THE PHOTOGENERATION OF HYDROGEN GAS

BY

Charles A. Ayotte IV

BS, Rochester Institute of Technology, 2015

THESIS

Submitted to the University of New Hampshire

in Partial Fulfillment of the Requirements for the Degree of

Master of Science

in

Chemistry

September 2018

This thesis/dissertation has been examined and approved in partial fulfillment of the requirements for the degree of Master of Science in Chemistry by:

Thesis Director, Christine Caputo,
Assistant Professor of Chemistry

Roy Planalp,
Associate Professor of Chemistry

John Tsavalas,
Associate Professor of Chemistry

On July 18, 2018

Original approval signatures are on file with the University of New Hampshire Graduate School.

ACKNOWLEDGEMENTS:

Firstly, I would like to thank my research advisor, Dr. Christine Caputo for the encouragement and guidance throughout this project. Her go-getter attitude has been and continues to be inspiring.

I would like to sincerely thank my friends and colleagues at UNH, Hannah Bell, Elizabeth Bright, Jonathan Fifer, Samantha Gillingham, Conor Gomes, Carter Holt, Ethan Jarvis, Brian Patenaude, Zane Relethford, and Stacie Stuut for their continued comfort and excitement. You have all become such wonderful friends and I am grateful to have worked closely with each of you.

Many thanks to my family for their endless reassurance and support. I have been able to accomplish so much thanks to all of you. May you continue to be an inspiration for my success.

To my RIT family, you have all been and continue to be the catalyst for my growth and I cannot thank you all enough for that. May we never stop sharing our adventures and continue to push each other to greatness.

And last but certainly not least, I'd like to send a thanks to the hip-hop community for providing the soundtrack to my journey and serving as an outlet throughout my doubts.

TABLE OF CONTENTS:

ABBREVIATIONS:

2D – two-dimensional

AA – ascorbic acid

AcOH – acetic acid

AFM – Atomic Force Microscopy

BP – Black Phosphorus

BPQD – Black Phosphorus Quantum Dot

CAISO – California Independent System Operator

DLS – dynamic light scattering

DMA – dimethyl aniline

DMF – dimethylformamide

DMSO – dimethylsulfoxide

EDTA – ethylenediaminetetraaceticacid

FEP – fluorinated ethylene propylene

GC – gas chromatography

HRTEM – High Resolution Transmission Electron Microscopy

ICP-MS – Inductively coupled-mass spectroscopy

IPA – isopropyl alcohol

KXan – potassium xanthogenate

MeCN – acetonitrile

MV – methyl viologen

NHE – Normal Hydrogen Electrode

nIR – near infrared

NMP – N-methyl-2-pyrrolidone

Ox. Cat. – Oxidation Catalyst

PEG – polyethylene glycol

Pt@citrate – citrate capped platinum nanoparticles

PV – Photovoltaic

QD – Quantum Dot

Red. Cat. – Reduction Catalyst

SED – sacrificial electron donor

SEM – Scanning Electron Microscopy

TBAHSO4 – tetrabutylammonium hydrogensulfate

TCD – thermal conductivity detector

TEA – triethyl amine

TEM - Transmission Electron Microscopy

TEOA - triethanolamine

TMD - Transition Metal Dichalcogenide

UV - Ultraviolet

vis - Visible

XPS - x-ray photoelectron spectroscopy

LIST OF FIGURES

LIST OF TABLES

ABSTRACT:

BLACK PHOSPHORUS QUANTUM DOTS: SYNTHESIS, CHARACTERIZATION, AND UTILIZATION TOWARDS THE PHOTOGENERATION OF HYDROGEN GAS

By

Charles A. Ayotte IV

Black phosphorus (BP) is a semiconducting allotrope of phosphorus that forms buckled 2D layers. Originally discovered by Percy William Bridgman in 1914,[1] the research community mostly ignored this material until 2014 when unexplored properties and applications became more apparent. This resurgence in interest in this material is being dubbed the "renaissance of black phosphorus".[2]

Black phosphorus find itself alongside the likes of graphene in an interesting category of materials known as layered semiconductors.[3] These 2D materials are characterized by strong intralayer covalent bonds and weak interlayer Van der Waals forces. Since these interlayer forces are so weak, single or few layers of these materials can be isolated in nanoflake or nanoparticle form (sometimes referred to as a quantum dot) and express different properties than their bulk counterparts. For example, black phosphorus has a tunable band-gap, dependent on its layer count, that ranges from 0.3-2.0 eV.[4,5] This bandgap sits right between the experimentally

observed bandgaps of graphene and TMDs.[6] These types of properties are of interest for the photocatalysis community.

Despite recent advances in generating and utilizing BP materials for photocatalytic systems there are still a few successes utilizing black phosphorus quantum dots (BPQDs) and a co-catalyst. Quantum dots offer electronic and morphology differences compared to their nanoflake counterparts. BPQDs have been shown to have stronger absorption of solar light and larger surface areas which lead to more efficient photocatalysis.[7] Modified BP systems using co-catalysts and surface functionalization for the photogeneration of hydrogen gas have been explored in systems using BP nanoflakes but, a modified BPQD system has yet to be reported.

Platinum is a commonly employed and well-studied catalyst for the reduction of protons to hydrogen gas since it's conduction band is lower than most photosensitizers while being high enough to still efficiently drive the reaction.[8] The reduction of platinum onto other surfaces or to form nanoparticles can be easily achieved. For example, either H_2PtCl_6 or K_2PtCl_6 can be chemically reduced by $NaBH_4$ in the presence of a capping agent like citric acid to produce platinum nanoparticles that will not aggregate for months.[9] This reduction has also been carried out using photo-activated semi-conducting material as the reducing agent resulting in the platinum precursor to form nanoparticles on the surface of the semi-conductor.[10]

Herein, a system utilizing BPQDs and platinum nanoparticles for the photo-production of hydrogen gas will be presented. BPQDs were synthesized from bulk BP crystals via ultrasonication liquid-exfoliation in NMP. BPQD particle size and

morphology was explored through SEM and AFM imaging techniques. Photo-physical properties of BPQDs was observed through UV-vis spectroscopy, fluorescence spectroscopy, and methyl viologen based "electron transfer probe" experiments. Colloidal platinum nanoparticles were synthesized through the chemical reduction of H_2PtCl_6 via $NaBH_4$ in the presence of citric acid. Platinum was also photochemically reduced by BPQDs to produce a composite BP-Pt material. The photocatalytic capabilities of BPQDs in the presence of colloidal platinum nanoparticles and surface bound platinum were compared. Alternative strategies to achieving hydrogen fuel generation using BPQDs is discussed.

1 INTRODUCTION

1.1 A CALL FOR INNOVATION IN RENEWABLE ENERGY

Due to advancing technology and rising populations the energy demand of the United States has risen dramatically in the past half-century. Thanks to some of the technological innovations of recent times, however, energy demands have started to level off.[1] Sustainability concerns over the use of fossil fuels have caused a shift in sources of energy production with renewable energy and natural gas seeing the largest increases.[2] While this increased use of renewable energy sources has been beneficial for reducing our use of carbon-intensive fuels, they have introduced a new set of problems for energy grids.

An interesting example of these problems was highlighted in 2013* when California Independent System Operator (CAISO) first published a chart showing the potential for "overgeneration" of energy due to increasing numbers of photovoltaic (PV) cells being installed and utilized. A graph published by CAISO, referred internally as "The Duck Chart", shows the energy demands for California on a typical spring day for the years of 2012 and 2013 with predicted demands for 2014-2020 (Figure 1). Due to the decreasing demands during sunlight hours, there is an increasing lull from ~ 8 am - ~ 5 pm but an increasing peak that spans from ~ 7 pm - ~ 9 pm. This pattern requires a huge ramp in energy production that plants are

* Note: these resources were updated since their initial release

finding harder and harder to deal with. Many plants have shifted to overproducing energy during the day, which ultimately gets wasted, to reduce the need to ramp production so quickly to meet peak needs.[3]

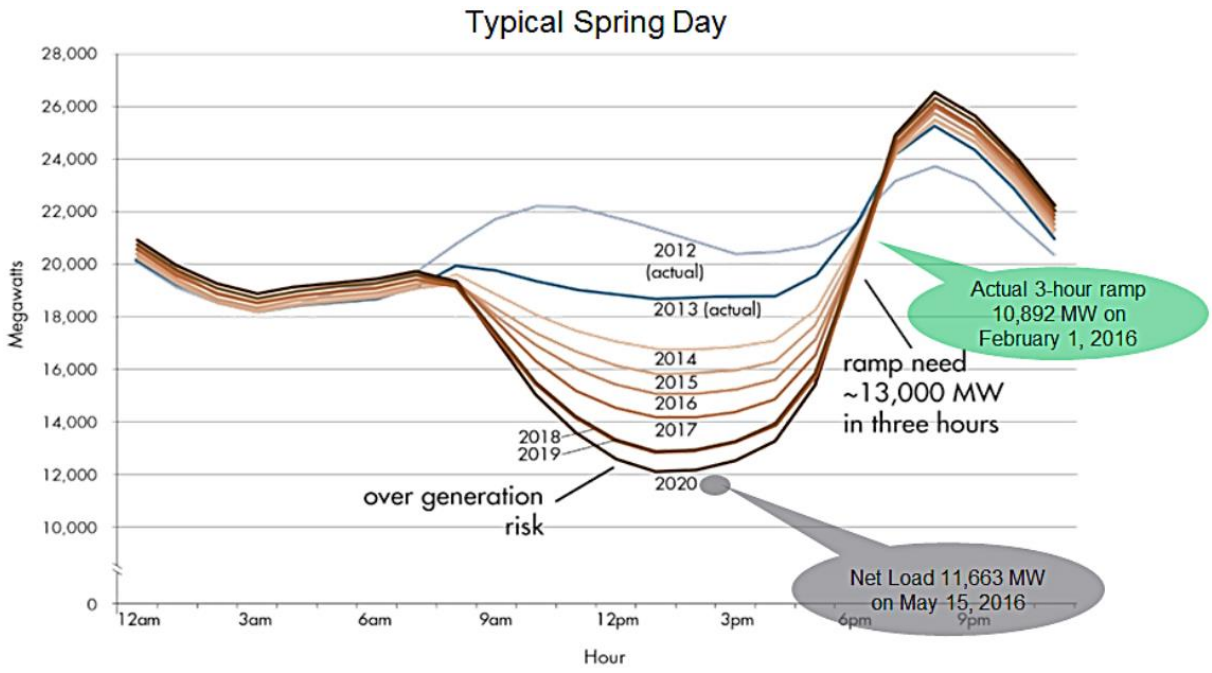

Figure 1: The Duck Chart; Power demands within an energy plant on a typical spring day in California that shows increased ramping needs as the years progress.

While this problem continues to grow CAISO proposes several answers to this problem, with one answer succinctly suggesting "better energy storage". Batteries are often the first technology people think of when it comes to energy storage but, as Dr. Kuzhikalail M. Abraham of Northeastern University discusses in his piece published in The Journal of Physical Chemistry Letters: "Advanced Li-ion batteries may not be able to meet this challenge in the near term" due to physical and chemical constraints.[4] However, many scientists have been looking at storing energy in

chemical bonds, a field of research being called solar fuels generation or artificial photosynthesis.

1.2 HYDROGEN AS A PROMISING, SOLAR-DERIVED FUEL

Many researchers are interested in utilizing sunlight because of the near inexhaustible amount of energy it could provide. Energy equal to "about 10000 times the global energy demand"[5] hits the Earth every day. If we could efficiently harvest a fraction of that energy we meet our ever-increasing energy needs easily. Converting sunlight to electricity via PV technology has and continues to be useful but, as outlined earlier it is not a complete answer for our energy needs. The process of capturing that energy to synthesize a fuel is becoming a very attractive addition to our solar utilization.

Rather than developing new fuels, solar fuels researchers are targeting feedstocks like hydrogen and simple carbon-based molecules that are already established for industrial use.[6] This allows us to avoid having to develop new infrastructure for the storage, transport, and consumption of these products. Currently, methods for producing many of these feedstocks requires a lot of energy and often have harmful byproducts.[7]

Specifically, hydrogen is showing promise not only as an industrial feedstock but also as an alternative to fossil fuels. Hydrogen can be used in a fuel cell to electrochemically convert the chemical energy into both electrical work in the form of a current and heat (Figure 2). Most fuel cells are comprised of the same three major

components; an anode, an electrolyte channel or membrane, and a cathode. Fuel can enter the cell through an inlet to interact with an anode where a catalyst, typically a metal oxide,[8] converts the fuel to protons and electrons. These electrons are transferred through a wire, generating a current, while the protons move through an electrolyte or membrane where they both meet up at the cathode. At the cathode a separate catalyst, typically platinum based,[9] combines the protons, electrons, and oxygen to produce water and heat. The heat and current produced during this process are utilized to drive whatever device or machine the cell needs to power. Since the only other product produced in this method is water, which is easy to remove and safe to the environment, this is considered a zero-emission process.

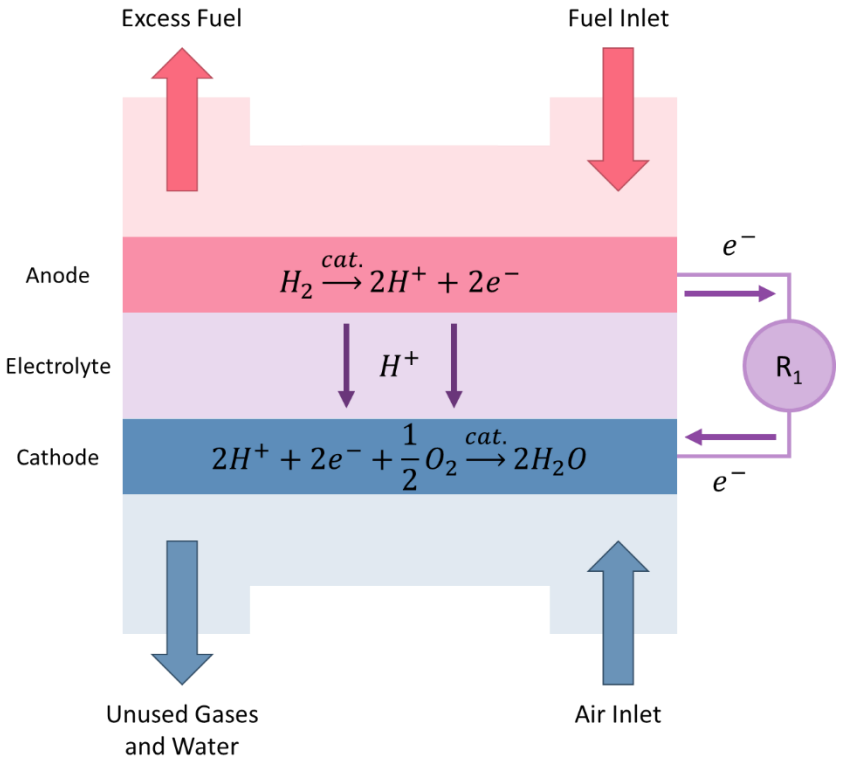

Figure 2: Schematic Illustration of a Hydrogen Fuel Cell

This technology is mostly being used in the automotive industry as transportation alone is responsible for ~17% of global greenhouse gas emissions.[10] Fuels cells could offer a much cleaner alternative while showing examples of almost doubling the efficiency of traditional combustion engines.[11] While recently there has been a large focus on battery powered vehicles, the emerging market of fuel cell electric vehicles expected to account for nearly 70,000 vehicles by 2027.[12,13] As of 2018 there are currently only three models commercially available in select markets; Toyota Mirai, Hyundai ix35 FCEV, and Honda Clarity.

While hydrogen is one of the most abundant chemical substances in the universe it is scarcely found on Earth since it readily escapes Earth's gravity due to its low molecular weight.[14] For this reason, hydrogen production is one of the most important hurdles before the adoption of hydrogen as an alternative fuel. Presently, the most common ways to produce hydrogen is through steam reforming of hydrocarbons and electrolysis of water.

According to the U.S. Department of Energy steam reforming is responsible for nearly 95% of all hydrogen produced in the United States.[15] Most commonly this is done through the steam-methane reforming process (Figure 3, top) in which methane and water are heated to over 700°C – 1,000°C and reacted under 3-25 bar pressure in the presence of a catalyst to produce hydrogen and carbon monoxide. Following this is

Steam-methane reforming reaction:

$$CH_4 + H_2O + heat \xrightarrow{catalyst} CO + 3H_2$$

Water-gas shift reaction:

$$CO + H_2O \xrightarrow{catalyst} CO_2 + H_2$$

Figure 3: Steam Reforming Reactions

the “water-gas shift reaction” (Figure 3, bottom) in which the carbon monoxide is reacted with more water to produce carbon dioxide and more hydrogen gas. While this process produces hydrogen in large quantities it requires immense amounts of heat to begin and produces carbon dioxide, a leading factor for climate change. These factors are slowing the acceptance of hydrogen as a “cleaner” alternative to fossil fuels.

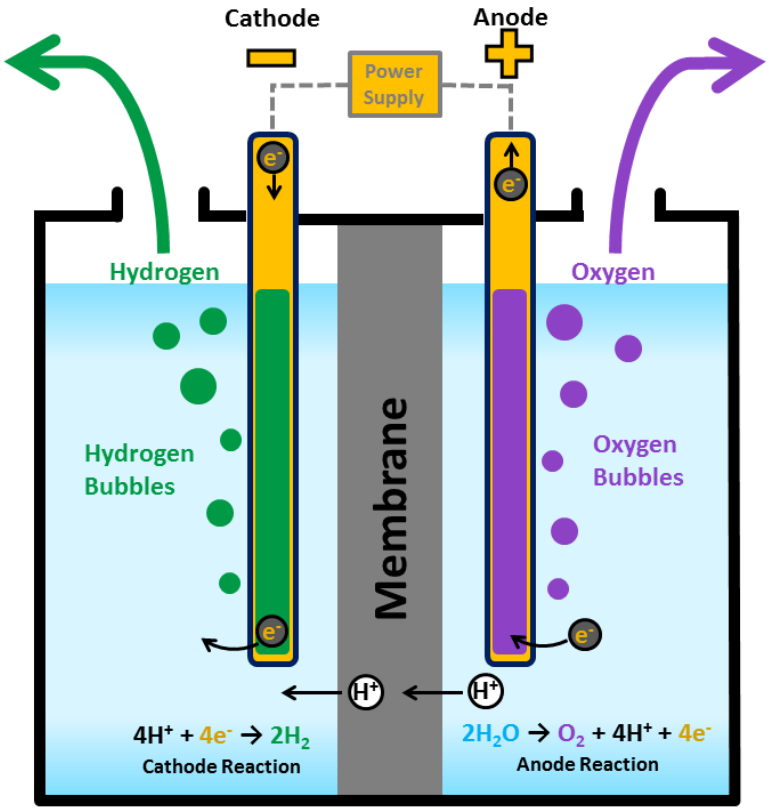

Figure 4: Schematic illustration of water electrolysis[16]

The electrolysis of water does not account for nearly as much of the hydrogen produced in the U.S. due to large energy requirements and currently inefficient design. The overall process of electrolysis (Figure 4) can be separated into two main reactions, the oxidation of water and the reduction of protons, both being driven

thermodynamically by a bias applied to separate electrodes to carry out each reaction. Water oxidation transforms water into molecular oxygen, protons, and electrons whereas proton reduction combines those protons and electrons to create molecular hydrogen. While the processes can occur in the same vessel, it is best to include a gas-impermeable membrane to separate the gases produced as oxygen and hydrogen will favorably react with one another to reproduce water bypassing the goal of this process. Conveniently, this process can be powered by alternative energy sources such as the previously described PVCs allowing hydrogen gas to act as a chemical storage of the energy harnessed through the sun. However, this process is thermodynamically demanding, requiring a theoretical 34 kWh/kg of hydrogen generation and current models requiring ~50kWh/kg to operate.[17] The kinetic requirement of transferring 4 equivalents of protons and electrons also makes electrodes difficult to design.[18] This all leads to high cost and energy demand limiting the widespread use of electrocatalytically splitting water.

1.3 Solar Fuels & Hybrid Photocatalysis

Luckily, nature has provided ample inspiration into how we may be able to produce fuels efficiently using sunlight. For example, through photosynthesis, plants, algae, and various bacteria have been shown to absorb sunlight and convert water and carbon dioxide into oxygen and carbohydrates. These carbohydrates are later used like fuels to power processes throughout the organism. Research aimed at mimicking these sorts of processes has been dubbed artificial photosynthesis. Instead of a bias powering these systems, they use a light harvesting system that captures

and converts solar energy into the redox potentials required for driving chemical reactions. A few common chemical reactions that produce solar fuels and their redox potentials, converted to NHE reference and pH=7,[19] are as follows:

$2H_2O \rightarrow O_2 + 4H^+ + 4e^-$	+0.81 V	(1)
$2H^+ + 2e^- \rightarrow H_2$	-0.42 V	(2)
$CO_2 + 2H^+ + 2e^- \rightarrow HCOOH$	-.061 V	(3)
$CO_2 + 2H^+ + 2e^- \rightarrow CO + H_2O$	-0.53 V	(4)
$CO_2 + 4H^+ + 4e^- \rightarrow HCHO + H_2O$	-0.48 V	(5)
$CO_2 + 6H^+ + 6e^- \rightarrow CH_3OH + H_2O$	-0.38 V	(6)

Before considering which materials might fit the bill, it's important to understand what happens at the chemical level in these systems. While there are several different mechanisms that can be followed, dependent on the exact combination of materials, they all follow the same basic steps (Figure 5).

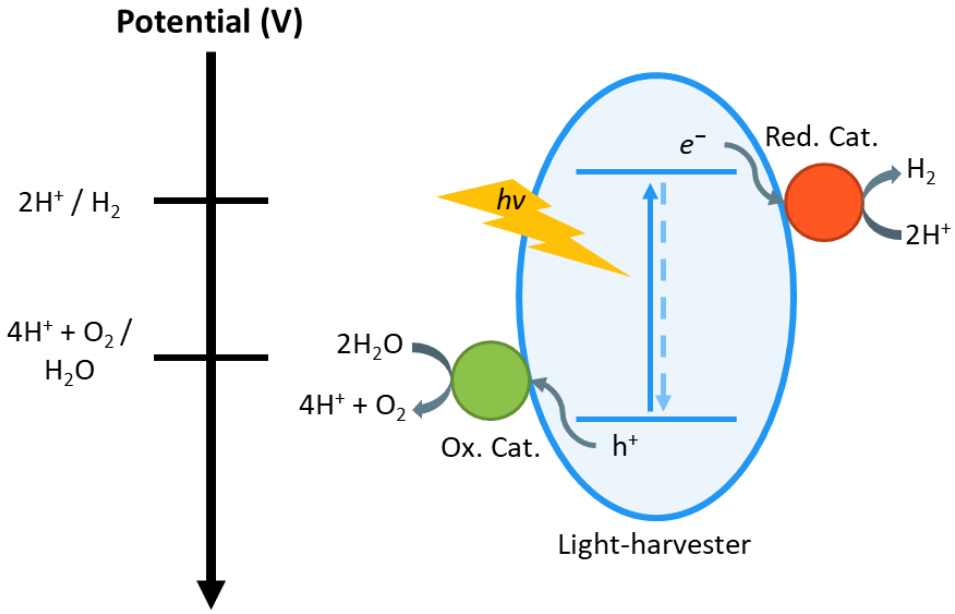

Figure 5: Energy diagram depicting the harvesting of solar energy, charge separation, and electron transfer processes of a hybrid photocatalytic system

First, the light harvester absorbs a photon of an energy level that matches its bandgap, allowing for the excitation of an electron from its valence band to its conduction band, creating an electron-hole pair. In this excited state, the electron can then travel downhill in energy to a substrate, usually a target molecule or a reduction catalyst (Red. Cat), to perform the desired chemical reduction reaction. To replenish the cycle a third component, either an oxidation catalyst or target electron donor, can accept the generated hole to perform the desired oxidation reaction. It should be noted that these redox reactions are commonly studied separately, by adding in sacrificial donor agents that can be oxidized or reduced in place of one of the catalyst centers, to better isolate what is happening at each site. However, to produce systems that will be commercially viable these reactions will need to be properly paired in practice.[20]

The performance of these hybrid systems is determined both by the properties of the individual components and the interaction between these components under the experimental conditions. Therefore, there are several factors that must be considered when designing novel systems. For example, thermodynamically, the redox potentials of each component need to be aligned such that the light harvester can generate an electron-hole pair that can be transferred to catalysts that have potentials capable of driving the desired chemical transformations. However, thermodynamics will determine if the catalysis is possible, but it is not as good at predicting overall efficiency.[21] It is also important to consider the optical and electrochemical properties of the light harvester in the system very carefully. Ideally this component should be able to absorb photons from a broad range of wavelengths that make the most of the

solar spectrum with a high molar extinction coefficient, have stable enough excited states that allow for electrons/holes to transfer before recombination occurs, and be stable enough for multiple reduction-oxidation cycles.[22]

These targets for light harvesters have led to researchers employing a variety of materials such as organic dyes[23], organometallic complexes[24], and semiconductors.[25,26] Metal-based dyes, like ruthenium polypyridines and porphyrins, can absorb light via several transitions that can be metal-centered or involve metal-to-ligand or ligand-to-metal charge transfers. These complexes tend to be more photostable due to the redox stability of the metal center.[27] Organic dyes are comprised of less-expensive, more-abundant elements and tend to have higher extinction coefficients and their absorption is often due to $\pi \rightarrow \pi^*$ transitions. However, these molecules are prone to degradation and/or aggregation under catalytic conditions hindering their long-term stability.[28] Light harvesting semiconductors offer some new properties to hybrid photocatalytic systems compared to their molecular counterparts such as strong electron transport properties and can act as physical scaffolds. Semiconductors with narrow bandgaps absorb visible light well without the addition of auxiliary dyes but often suffer from instability in water. Wider band-gap semiconductors tend to be more stable but only absorb in the UV limiting their solar efficiency. Dye-sensitized semiconductors have been utilized to have the advantageous stability of semiconductors combined with the stronger visible light utilization of organic dyes and have been reviewed recently.[20] In the interest of avoiding toxic and/or expensive materials however, researchers have started looking

towards non-metal-based semiconductors such as graphene, carbon nitride, and elemental semiconductors like black phosphorus.[29]

1.4 History and Properties of Black Phosphorus

Black phosphorus (BP) is a semiconducting allotrope of phosphorus that forms buckled 2D layers (Figure 6)[30]. Originally discovered by Percy William Bridgman in 1914,[31] the research community mostly ignored this material until 2014 when unexplored properties and applications became more apparent. This resurgence in interest in this material is being dubbed the "renaissance of black phosphorus".[32]

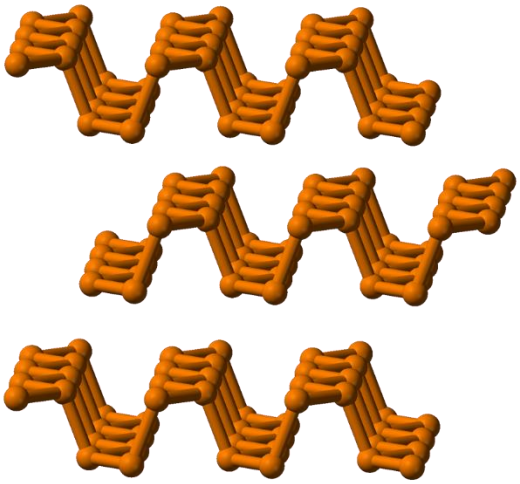

Figure 6: Structure of BP displaying puckered layers

Black phosphorus find itself alongside the likes of graphene in an interesting category of materials known as layered semiconductors.[33] These 2D materials are characterized by strong intralayer bonds and weak interlayer Van der Waals forces. Since these interlayer forces are so weak, single or few layers of these materials can be isolated in nanoflake or nanoparticle form (sometimes referred to as a quantum dot) and express different properties than their bulk counterparts. For example, black phosphorus has a tunable band-gap, dependent on its layer count, that ranges from 0.3-2.0 eV.[34,35] This bandgap sits right between the experimentally observed bandgaps of graphene and TMDs.[36]

Due to these unique properties, there is a lot of interest in using these types of materials as photosensitizers in photocatalytic experiments. 2D materials in general offer advantages compared to other photosensitizers that include increased stability and greater tunability, and metal-free 2D materials also have the benefit of often being non-toxic.

As promising as black phosphorus seems, there are a few limitations to its widespread use that are still being addressed. Although it is the most thermally stable allotrope of phosphorus, it is still susceptible to degradation in the presence of water, oxygen, and light. A solution involving the large-scale protection of black phosphorus is still being developed. The observed degradation products for BP are various biocompatible phosphorus oxides such as phosphoric acid.[37]

1.5 Generation, Isolation, and Characterization of Black Phosphorus Quantum Dots

Researchers first sought to efficiently exfoliate bulk black phosphorus into flakes and quantum dots. Luckily, many researchers have already shown great success in exfoliating graphene samples allowing black phosphorus researchers to adapt their methods. The most common method for exfoliation black phosphorus is liquid exfoliation through ultrasonication. In general, this method involves grinding bulk black phosphorus and adding it to a solvent and then sonicating using a variety of sonicators. This method produces nanoparticles and/or nanoflakes depending on sonication power, and time. A review of currently reported liquid exfoliation techniques for BP was recently published.[38]

Chu and colleagues showed that to achieve the smallest most regularly shaped black phosphorus dots they needed to employ both a bath and probe sonicator. They were able to make this conclusion by drop casting the resulting suspension of black phosphorus material and imaging the samples through TEM and AFM (Figure 7).[39]

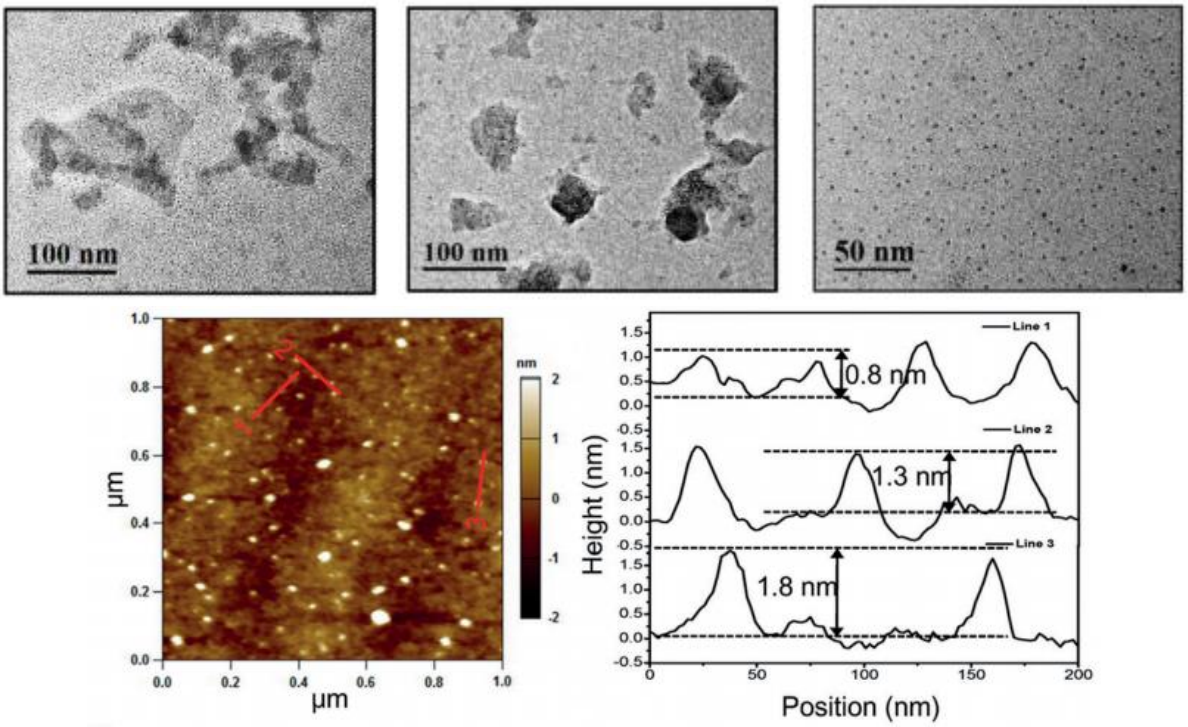

Figure 7: HRTEM images of BPQD samples produced via probe sonication (top-left), bath sonication (top-middle), bath and probe sonication (top-right). AFM image and height profiles of bath and probe sonicated sample (bottom)

It was also shown that sonication should be performed in highly viscous solvents such as N-methyl-2-pyrrolidone (NMP) to achieve suspensions with higher concentrations of BP. Warren and co-workers systematically explored 18 different organic solvents, including pyrrolidones, formamides, alcohols, and others containing phenyl rings, for their ability to create a suspension of exfoliated black phosphorus.[40]

These generated samples were then centrifuged using similar conditions, which will be explored later, to isolate the few-layer BP material in each solution, and redispersed in fresh solvent. Inductively coupled-mass spectroscopy (ICP-MS) and UV-vis-nIR spectroscopy were correlated to determine the concentration of BP in each sample.

This analysis showed that while there was a lot of solvent-to-solvent variability there were a few solvents, including NMP, that could produce solutions of significantly higher concentration. It was theorized that the viscous solvents allowed the better transfer of the sonication power and may have prevented gases from interacting with the black phosphorus during sonication. This work also compared computationally calculated Hansen solubility parameters for each solvent to determine how each solvent was interacting with BP. There was no clear correlation between these parameters and the concentration of generated BP but, the authors suggest that these parameters could be used to explain why some solvents can yield high concentrations of BPQDs through sonication but, do not produce suspensions that last for as long as those reported for NMP.

While most work focusing on making BPQDs uses sonication methods like the ones already described, others have considered using alternative devices to generate enough force to exfoliate BP. Using a kitchen blender Zhu and colleagues synthesized BPQDs with an average size < 5 nm in size in only 0.66 h.[41] These researchers propose a mechanism for BPQD generation using this method that involves exfoliation into sheets followed by disintegration to QDs and is supported by TEM images taken of

intermediate samples over the course of blending (Figure 8). Alternatively, grinding via a ball-milling method was also shown to produce a BP powder made up of large, thin flakes.[42] However, it was observed that the ball-milling needed to be performed in the presence of a LiOH additive otherwise the BP would form unstable intermediates that would oxidize immediately upon exposure to air.

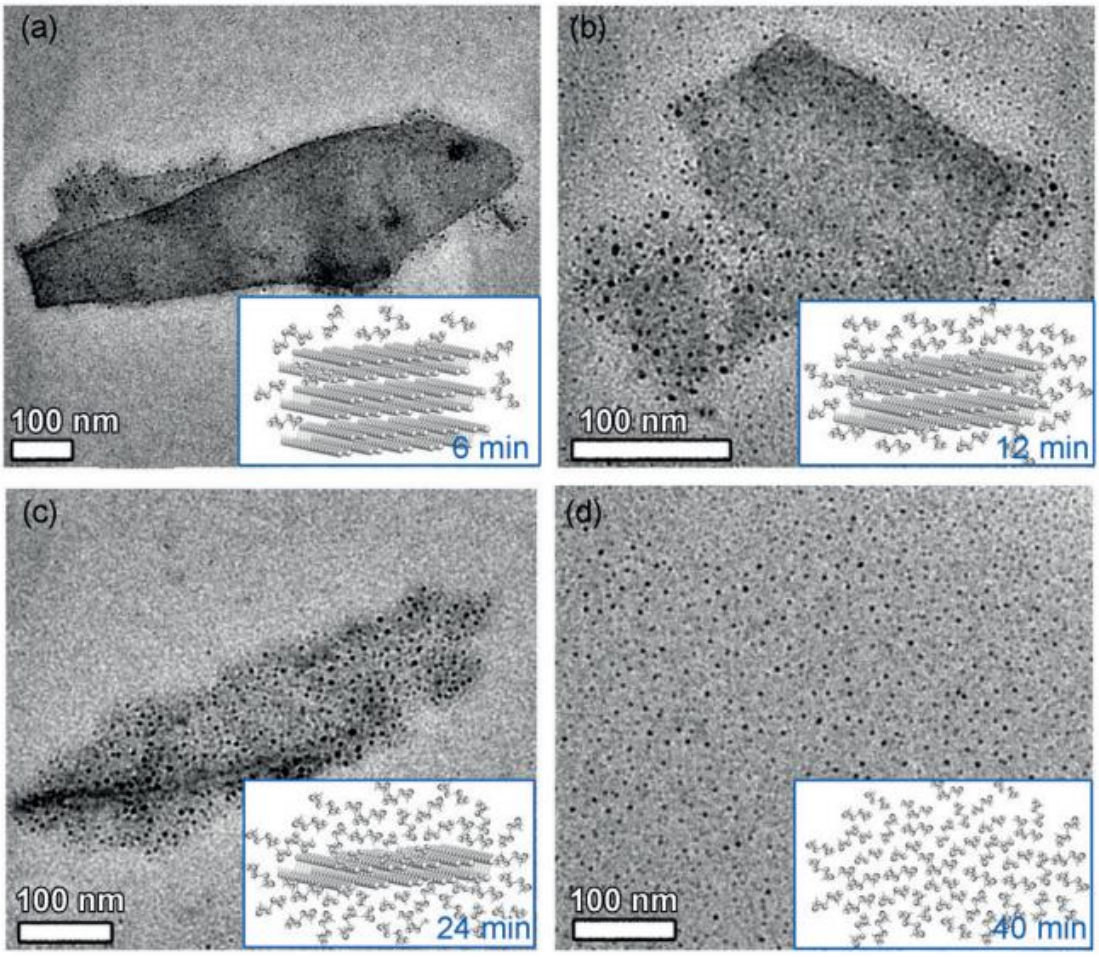

Figure 8: TEM images of blended BPQDs at different disintegration times.[41]

1.6 PHOTOCATALYSIS USING BLACK PHOSPHORUS

Research involving BP spans a variety of applications, of particular interest is their use in photocatalysis. The first reported used of BP as a photosensitizer was for the generation of singlet oxygen in August of 2015.[43] The authors claim their BP system achieved a calculated quantum yield of 0.91, placing it among some of the best photosensitizers for singlet oxygen generation. Interestingly, this work was one of the first to exfoliate BP in oxygen-free water for easier dispersion into water-based systems. The authors mention that their water-based samples were stable for more than 2 weeks, as determined by time-dependent XPS and Raman analyses, when kept in the dark but would quickly degrade when exposed to light. It was noted that it is known that NMP systems are stable for over a month, but the authors assumed that residual NMP would stay adsorbed onto the surface of the BP which could interfere with catalysis although this was not discussed any further.

In February of 2017 the first reported case of BP acting as a photocatalyst for the generation of hydrogen.[42] This group of researchers used a ball miller for mechanical exfoliation of BP and used LiOH as an additive for hydroxy functionalization of the BP flakes, as characterized by XPS, SEM, and TEM. SEM and TEM imaging showed that instead of quantum dots or pristine flakes that liquid exfoliation produces, their method produced a powder made up of aggregating thin flakes (Figure 9).

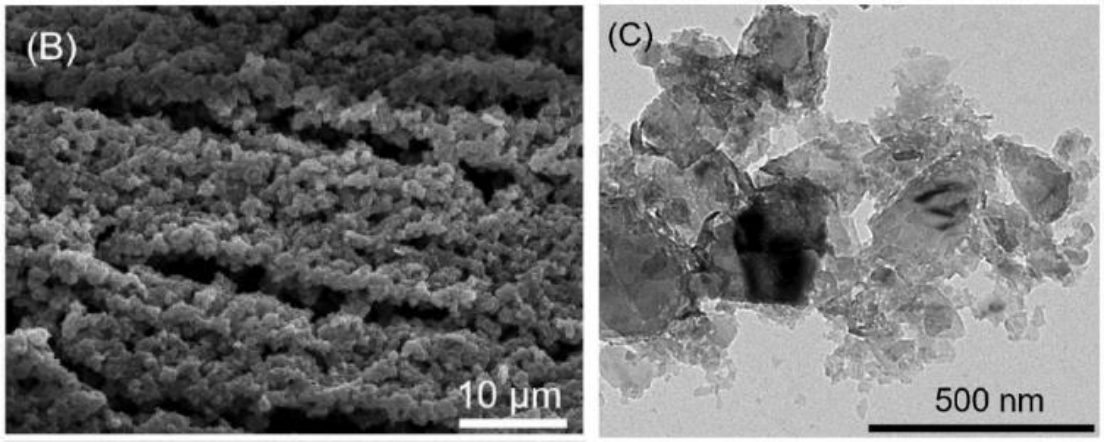

Figure 9: SEM image (left) and HRTEM image (right) of ball-milled BP.[42]

With these modifications in place they surveyed this material for H_2 evolution using Na_2S and Na_2SO_3 as sacrificial donors and a 300W Xe lamp with a UV cutoff (<420nm) filter attached. They reported a H_2 evolution rate of 512 μmol h^{-1} g^{-1} under these conditions. It should be noted that this reported hydrogen evolution rate is even higher than that of the more commonly used metal-free catalyst graphitic carbon nitride (g-C_3N_4), which was able to achieve 107 μmol h^{-1} g^{-1} with the addition of 3.0 wt% Pt.[44] This is incredible considering BP did not have a co-catalyst in this system. However, it is unclear if this stark difference is due to the electronic or morphology differences of the two materials.

Tian and colleagues also report an interesting system using BP supported CoP nanoparticles.[45] This composite material was synthesized via a solvothermal process using white phosphorus and ethylene diamine to create BP flakes and $Co(NO_3)_2 \cdot 6H_2O$ as a precursor for the CoP nanoparticles. CoP is an interesting co-catalyst considering it is the same noble-metal free, non-toxic catalyst used in Dan Nocera's water-splitting device; the "artificial leaf".[46] BP-CoP was able to achieve hydrogen

production in pure water without the need for any sacrificial agents. This system also represents a state-of-the-art quantum efficiency of 42.55% at 430 nm.

In October of 2017, the first un-modified-BP-based system for light driven hydrogen evolution was reported.[47] The group utilized liquid exfoliation to synthesize BP nanoparticles and nanoflakes and details a redispersion process to allow the BP to form a more stable suspension in acetonitrile as determined by UV-Vis measurements of their suspension after allowing the samples sit for several days. They were not able to uncover a mechanism for hydrogen evolution which they attribute to "low catalytic activity or phosphorus degradation".

1.7 Proposal For A Platinum Nanoparticle Assisted Black Phosphorus Quantum Dot Photocatalyst

Despite the recent advances in generating and utilizing BP materials for photocatalytic systems there were still a few successes utilizing BPQDs and a co-catalyst. Quantum dots offer electronic and morphology differences compared to their nanoflake counterparts. BPQDs have been shown to have stronger absorption of solar light and larger surface areas which lead to more efficient photocatalysis.[47] Modified BP systems using co-catalysts and surface functionalization for the photogeneration of hydrogen gas have been explored in systems using BP nanoflakes but, a modified BPQD system has yet to be reported.

Platinum is a commonly employed and well-studied catalyst for the reduction of protons to hydrogen gas since it's conduction band is lower than most photosensitizers

while being high enough to still efficiently drive the reaction.[48] The reduction of platinum onto other surfaces or to form nanoparticles can be easily achieved. For example, either H_2PtCl_6 or K_2PtCl_6 can be chemically reduced by $NaBH_4$ in the presence of a capping agent like citric acid to produce platinum nanoparticles that will not aggregate for months.[49] This reduction has also been carried out using photo-activated semi-conducting material as the reducing agent resulting in the platinum precursor to form nanoparticles on the surface of the semi-conductor.[50]

Herein, a system utilizing BPQDs and platinum nanoparticles for the photo-production of hydrogen gas will be presented. BPQDs will be synthesized from bulk BP crystals via ultrasonication liquid-exfoliation in NMP. BPQD particle size and morphology will be explored through SEM and AFM imaging techniques. Photo-physical properties of BPQDs will be observed through UV-vis spectroscopy, fluorescence spectroscopy, and methyl viologen based "electron transfer probe" experiments. Colloidal platinum nanoparticles will be synthesized through the chemical reduction of H_2PtCl_6 via $NaBH_4$ in the presence of citric acid. Platinum will also be photochemically reduced by BPQDs to produce a composite BP-Pt material. The photocatalytic capabilities of BPQDs in the presence of colloidal platinum nanoparticles and surface bound platinum will be compared. It is hypothesized that in-situ reduced Pt will outperform colloidal Pt due to the feasibility of electron transfer from BPQDs directly to Pt.

2 RESULTS & DISCUSSION

2.1 SYNTHESIS & CHARACTERIZATION OF BPQD SAMPLES

The first goal of this project was to determine the optimal conditions for synthesizing BPQDs via ultrasonication, with the primary solvent being *N*-methyl-2-pyrrolidone (NMP). NMP was chosen as the solvent of choice due to its high surface tension (42.61 mN/m) and established use as an exfoliation solvent for BP in the literature.[51] To accomplish this a series of samples were created using varying conditions such as amount of BP used, sonication method, sonication time, centrifugation speeds, centrifugation time. These samples were then characterized by a variety of methods. Imaging techniques including transmission electron microscopy (TEM), scanning electron microscopy (SEM), and atomic force microscopy (AFM) were used to gain information about the particle size and morphology of the exfoliated black phosphorus. Dynamic light scattering (DLS) was also used to gain information on particle size distribution in our samples. Inconsistencies were observed with this method that were derived from BPQDs photoactivity and irregular morphologies. Spectroscopic techniques like UV-Vis spectroscopy, and fluorimetry were used to gain knowledge about the photo-physical properties of these generated samples.

2.1.1 Optimization of sonication methods

The first samples created in this project were generated using different sonication tools, a probe sonicator and a bath sonicator. Sun and colleagues reported that it was

necessary to use both a 1200 W probe and 300 W bath sonicator to generate their "ultra-small" 5nm BPQDs.[39] These smaller BPQDs were of interest because their size would allow for a high relative surface area, which can allow for more atom efficient catalysis. To confirm these exfoliation results with our instruments, two samples were created, one using only a 100 W probe sonicator (CAA1-009) and the other using the probe and a 130 W bath sonicator (CAA1-07). Approximately 15mg of bulk BP crystals were added to 10mL of NMP. Both solutions were sonicated using a probe sonicator for 3 hours. CAA1-007 was also sonicated for an additional 6 hours using the bath sonicator. To remove the larger BP flakes that may still be present the solutions were centrifuged at 9000 rpm for 15 minutes. A wispy pellet is formed and the top 90% of the supernatant was collected and stored inside a glovebox.

Both samples were drop casted on silicon chips in a glovebox and later imaged via SEM. Since black phosphorus is semi-conducting no additional coatings were needed. Images generated from both samples showed a few similar features. Many of the particles in the sample were aggregated into clusters (Figure 10, top right). It was difficult however, for the instrument to generate sharply focused images on the smaller particles that were present in both samples. Despite these difficulties, it was still evident that these samples contained particles that were much larger than those reported by Sun and colleagues. This different result can be explained by the different powers of the sonicators used in this work. A particle size distribution for CAA1-009 was generated from DLS data (Figure 11).

2.1.1.1 Characterization for CAA1-007 and CAA1-009

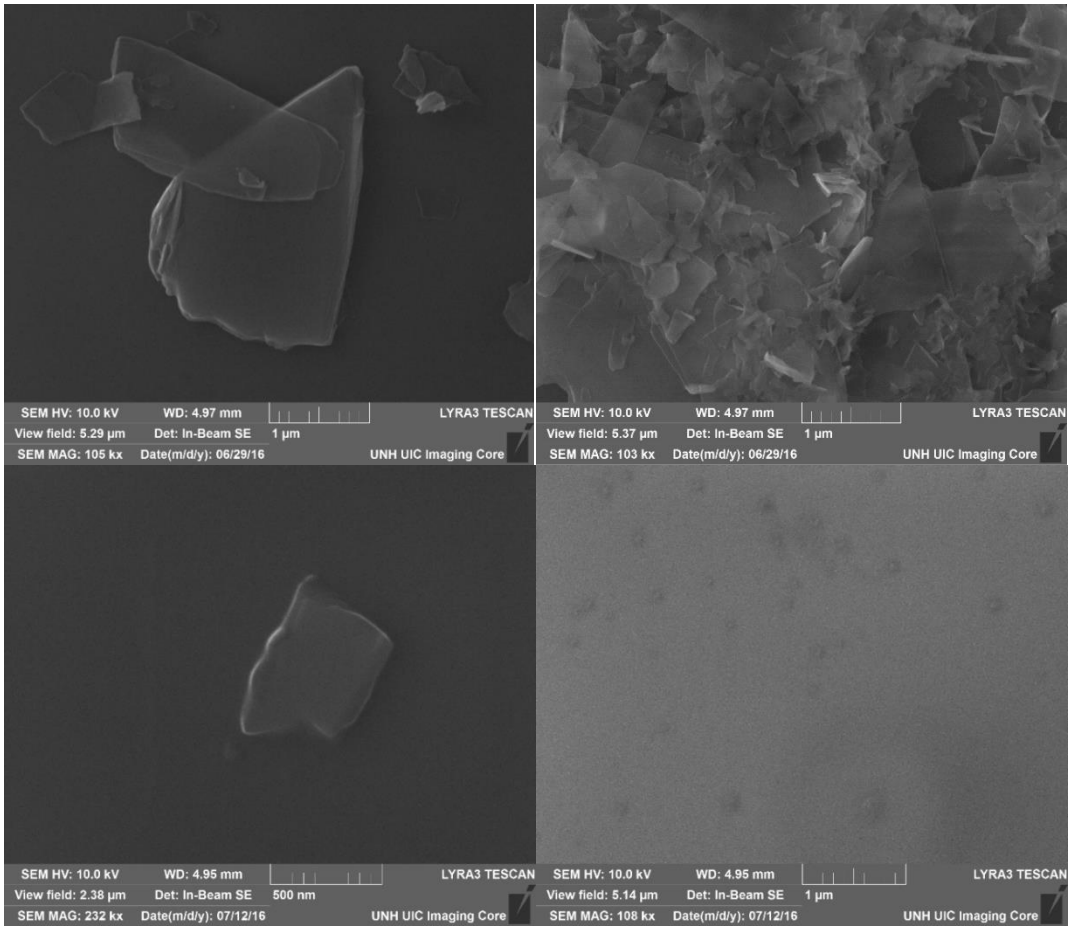

Figure 10: SEM images on a silicon chip of drop casted CAA1-007 (top), which utilized the probe sonicator, and of CAA1-009 (bottom), which utilized both the probe and bath sonicator.

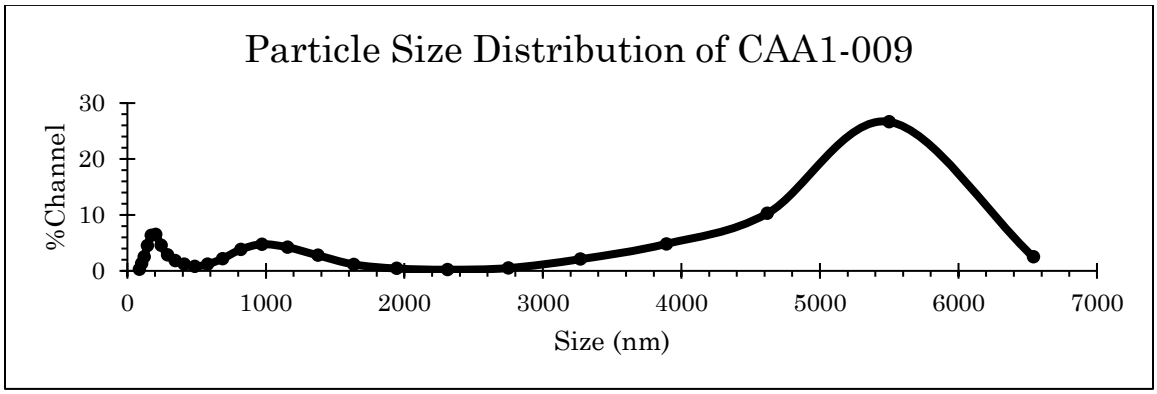

Figure 11: Particle Size distribution found in CAA1-009 generated via DLS

Previous methods discussed showed an abundance of larger flakes thus an attempt at generating smaller particles was made that employed ultrasonication with significantly longer sonication times. 15 mg of BP was combined with 10 mL of NMP in a glovebox and sonicated via the probe sonicator for 5 h and via the bath sonicator for 10 h. The solution was centrifuged at 9000rpm for 20 minutes and a very wispy pellet was observed. The top 90% of the supernatant was removed and stored in a glovebox (CAA1-016).

This solution was drop casted onto a silicon chip and the resulting sample was imaged via SEM (Figure 12). These images show a large population of large flakes about 1μm in size and a collection of significantly smaller size surrounding the large flakes. When trying to focus on the smaller, < 500 nm, flakes the instrument was having a harder time focusing as you can see in the increasing blurriness of the images.

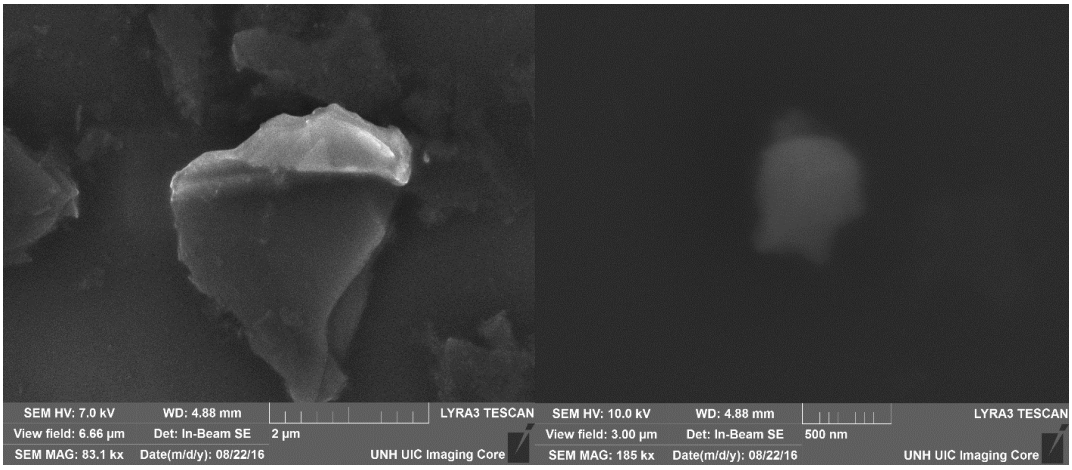

Figure 12: SEM images generated from CAA1-016

As DLS was providing inconsistent measurements when compared to our generated SEM images, an alternative method for determining particle size was sought. Atomic force microscopy (AFM) ended up being the method of choice due to the relative ease of use, and ability to measure the particle in three dimensions; height, width, and length. Sample preparation for AFM was identical to SEM preparation methodology so a portion of each sample was drop casted onto a silicon chip and imaged via AFM. (Figure 13) The height distribution of measured widths and heights of the particles observed is shown (Figure 14). The average particle width in this image was 63.3 ± 16.47 nm and the average particle height was 2.00 nm ± 1.08 nm which corresponds to ~4 ± 2 layers of BP as one layer of BP is about 0.5 nm.[32] This was the first data to confirm that few-layered black phosphorus nanomaterials were being generated using this sonication method. All BPQD solutions referenced herein were generated using these conditions.

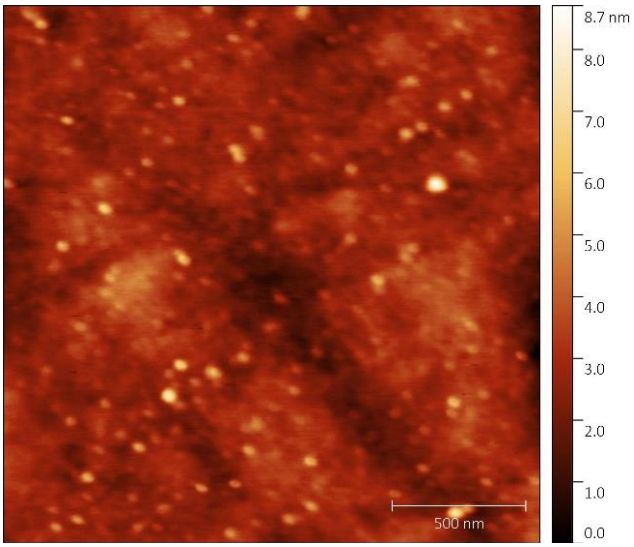

Figure 13: AFM Image generated from CAA1-016

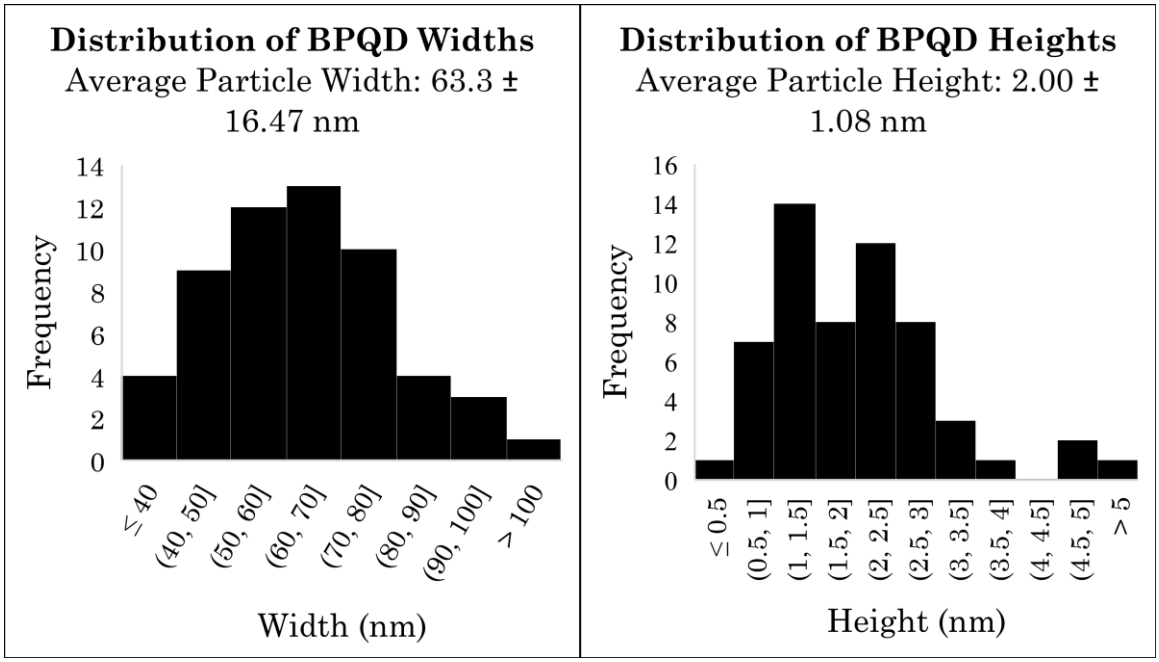

Figure 14: Particle size distributions with respect to width (left) and height (right).

2.1.2 Liquid Exfoliation of BPQDs using a Kitchen Blender

Considering the undesired results of previous attempts, alternative liquid exfoliation strategies were explored. Zhu and co-workers proposed a highly scalable method for creating BPQDs using a household kitchen blender.[41] Adapting their methods, 25 mg of bulk BP crystals and 250 mL of DMSO were added to a kitchen blender placed inside a fume hood. This combination was blended on the highest setting for 40 min. It was observed that during this blending period the plastic cap for the blender has begun dissolving in the DMSO. The resulting suspension was poured into a collection bottle and a 5.0 mL sample was placed into a teflon centrifugation tube. This sample was centrifuged at 9000 rpm for 15 minutes, no visible pellet was formed. The top 50% of the supernatant was collected (CAA1-011). A particle size distribution was obtained via DLS (Figure 15, left). This data suggests

that all the particles in this solution were less than 2nm but only a few data points were collected in that range. A portion of this sample was placed in a quartz cuvette to obtain a UV-Vis spectrum. No difference was observed between DMSO and the sample CAA1-011. For this reason, this method was deemed unsuccessful in producing BPQDs of a desired size or in a sufficient concentration.

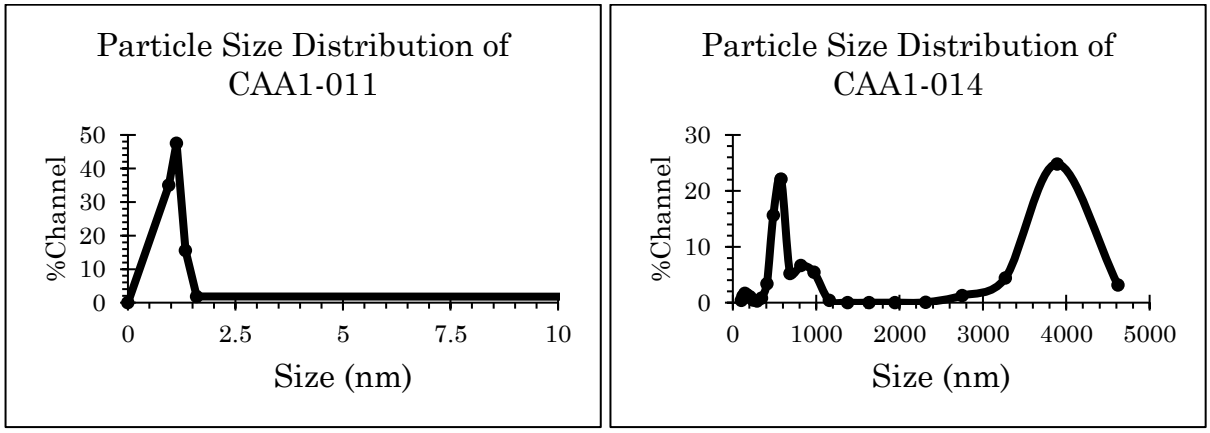

Figure 15: Particle size distribution of CAA1-011 (left) and CAA1-014 (right) determined via DLS

This method was modified before a second attempt to reproduce the results reported by Sun and co-workers. 30 mg of BP was weighed out and combined with 100 mL of DMSO inside the blender. Instead of using the plastic cap that came with the blender aluminum foil was used to cover the top of the blender. This solution was blended for 40 minutes, poured into a collection bottle, sealed, and then allowed to cool. A ~5mL portion of this solution was centrifuged at 9000rpm for 15 minutes and a small black pellet was observed. The top 50% of this sample was collected and labeled CAA1-014. A particle size distribution was generated using DLS (Figure 15, right). This data indicates that there was still a large portion of very large (>3μm) particles and a small population of particles ranging from 400 nm – 1000 nm.

Since DMSO is not a suitable solvent for drop casting due to the residue it leaves behind, redispersion of the BPQD into isopropyl alcohol (IPA) was performed. The DMSO solution containing BP was centrifuged at 12000 rpm for 30 min and a wispy pellet was formed. The top 90% of the supernatant was removed and replaced with IPA. This process of centrifuging and replacing the top 90% with IPA was repeated twice more. A sample for SEM imaging was prepared by drop casting the IPA solution onto a silicon wafer in a glovebox and allowing it to sit overnight. The images generated from this sample are shown (Figure 16). There were very large flakes that were well over 3 μm with a small population of tinier flakes also visible. These blended BPQD samples were not utilized further due to their undesirable results.

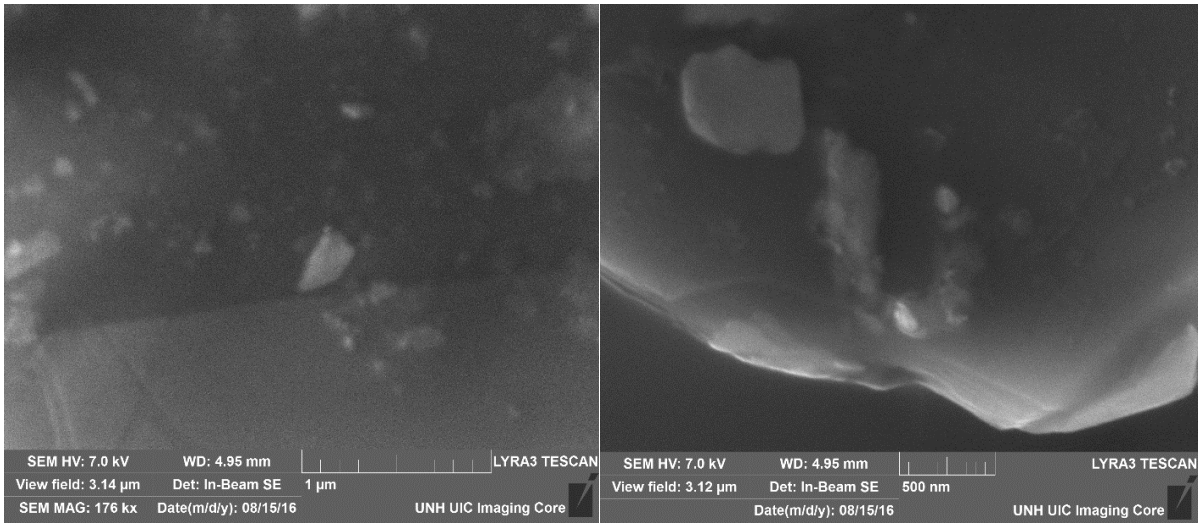

Figure 16: SEM images of drop casted BPQD solution CAA1-014

2.1.3 Passivation of BPQDs with polyethylene glycol

To allow BPQDs to be more water stable Sun and co-workers attached an amine terminated polyethylene glycol (PEG-NH_2) chain to the surface of BP.[39] However, the only evidence they offer to confirm this attachment is the observation that the BPQDs

to not crash out of aqueous solutions. There was no evidence to support N–P bond formation, so the authors claim the polymer chains were attracted to the surface due to electrostatic interactions. We sought to passivate the surface of our BPQDs using hydroxy terminated PEG-OH (Figure 17) as we expected the formation of a P–O bond to be easier than the formation of a P–N bond due to the thermodynamic strength of P–O bonds. The stretches of P–O–C bonding can also be observed via infrared spectroscopy and produce peaks around 1050 cm^{-1} and 845 cm^{-1} – 725 cm^{-1}.[52] Although, it is unclear how the electronics of BPQDs might affect these values.

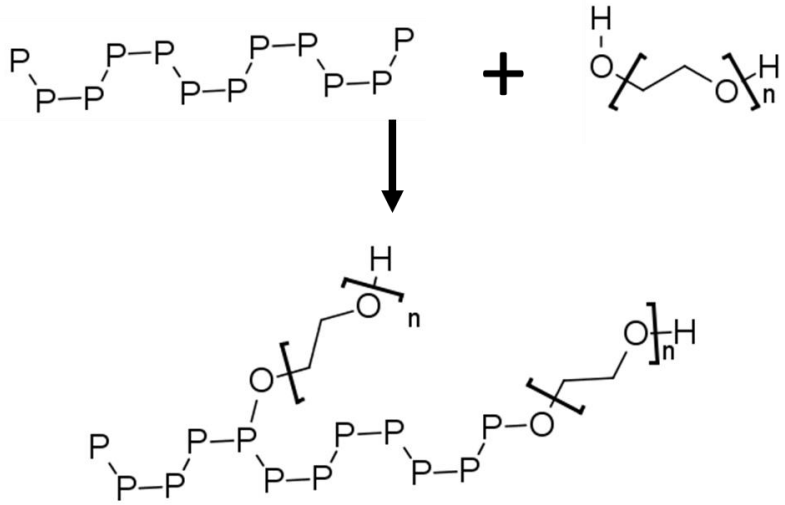

Figure 17: Molecular representation of expected bonding in PEG passivated BPQDs.

A portion of the BP-IPA solution generated previously was combined with 5 mg of PEG in a glovebox and then diluted to 10 mL of IPA before tightly sealing the vial. This mixture was sonicated for 30 min to ensure the BPQDs were properly suspended. The mixture was then stirred for 4 h and then labeled CAA1-015. This new solution

was measured via DLS to obtain the particle size distribution (Figure 18). It shows a polydisperse sample with suspended particles in the 40 nm – 400 nm range.

A portion of the PEG-BP sample was drop cast onto a silicon chip for SEM imaging. However, a charging phenomenon was observed (Figure 19, top). This occurs in SEM imaging whenever the electron beam is hitting a non-conductive material. This suggests the excess PEG-OH was still present and interfering with the images.

To remove the excess PEG, the solution was centrifuged at 12000 rpm for 20 min and the top 90% of the supernatant was replaced with IPA. This IPA suspension was then drop casted onto a silicon chip and imaged via SEM. This allowed for the generation of much clearer images (Figure 19). While there were still very large flakes present, these were not apparent in the DLS data, there were also a fair number of ~250 nm sized particles visible on top of the larger flakes.

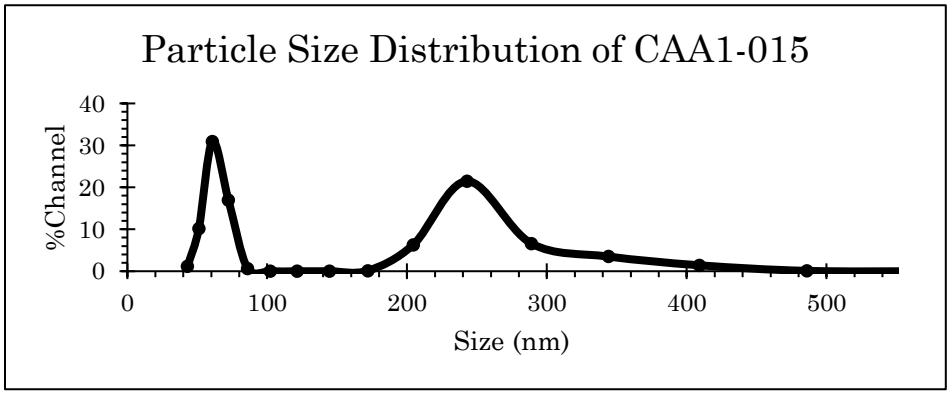

Figure 18: Particle size distribution for PEG-BPQDs (CAA1-015)

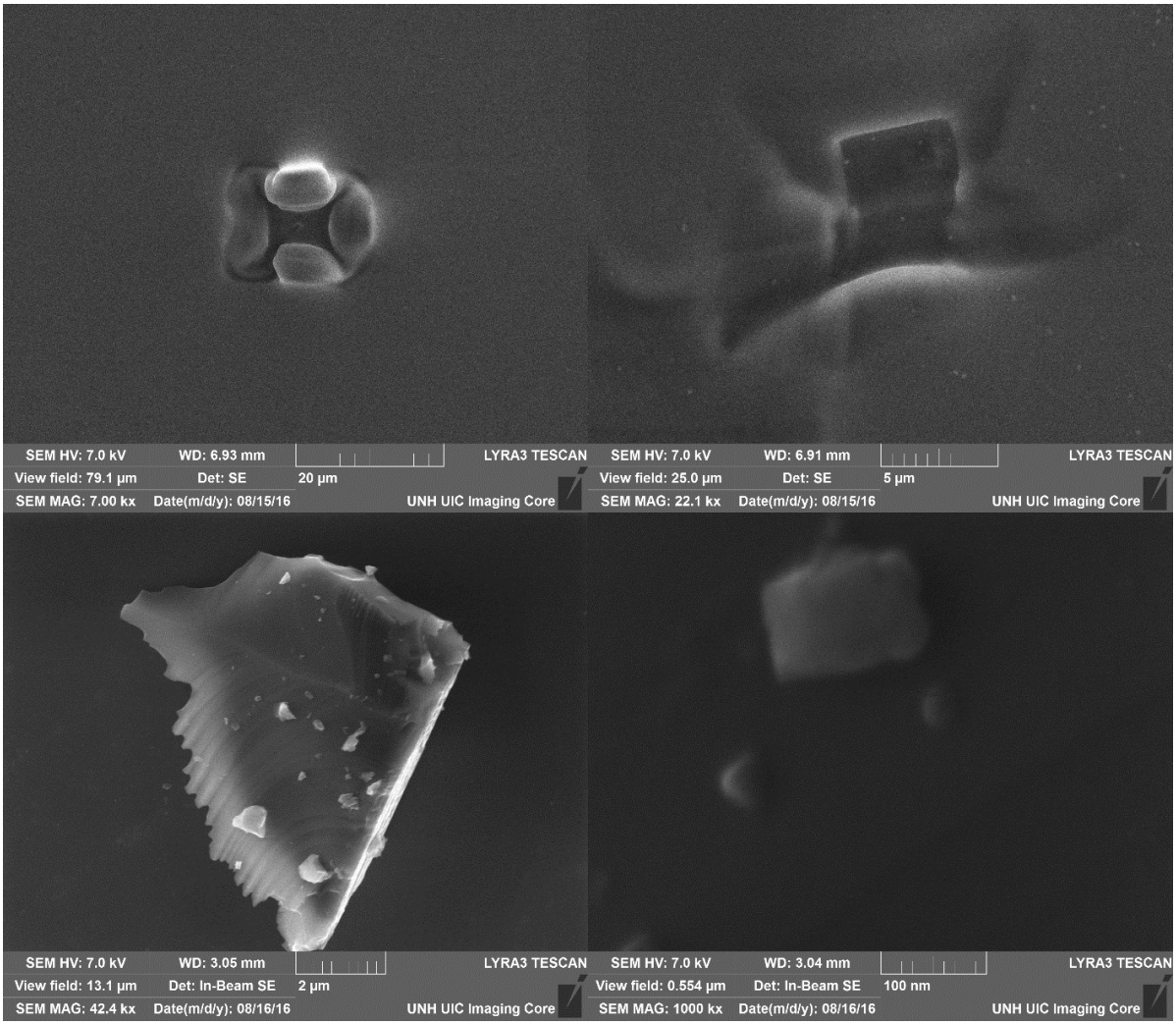

Figure 19: SEM images generated for CAA1-015. Top images show charging of some non-conductive material. Bottom images were taken after an IPA wash.

2.2 Understanding The Photo-physical Properties and Electron Transfer Capabilities of BPQDs

2.2.1 Photo-physical Properties of BPQDs

UV-vis spectroscopy was utilized to understand BPQDs ability to utilize the solar light spectrum (Figure 20). From this spectrum we can see that the standard BPQD solution makes good use of the visible range, a feature some semi-conductors struggle with.[53]

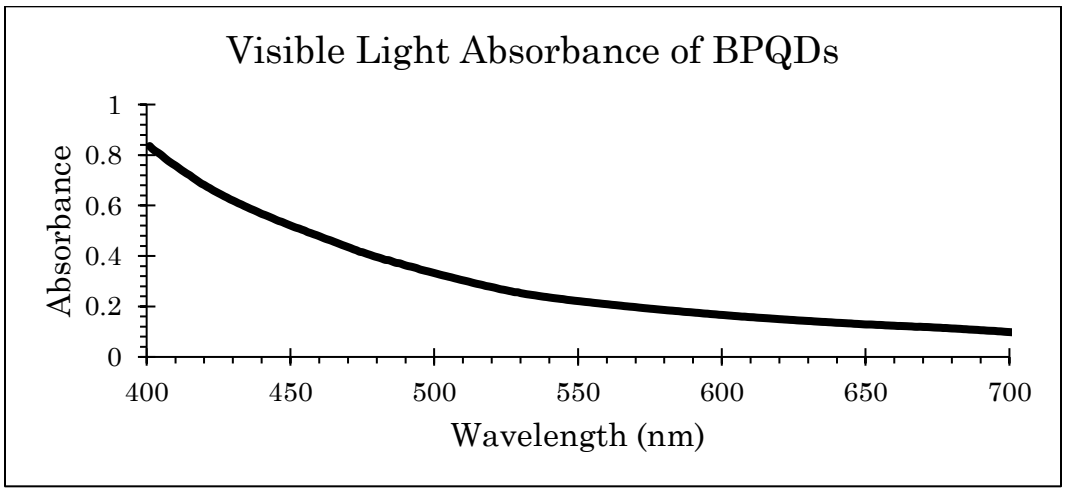

Figure 20: Visible light absorbance of standard BPQD solution in NMP

This data can also be used to make estimates about the concentration of BPQD solutions. Hanlon and colleagues were able to obtain the extinction coefficient, as well as the absorbance and scattering contributions, for BPQD solutions.[54] Using Beer's Law and an extinction coefficient, a concentration can be calculated. It was determined that at 465 nm the scattering effect of the particles contributes least to the extinction coefficient and is therefore the most accurate wavelength to base concentration calculations on. Using an absorbance coefficient of 15 mL mg^{-1} cm^{-1} a

BPQD concentration of 0.03 mg/mL was calculated for our standard BPQD solutions. It should be mentioned that without an instrument capable of separating absorbance and scattering contributions for our samples this number is a less accurate estimate.

Fluorescence spectroscopy was utilized to understand the photo-excitation of BPQDs (Figure 21). From this data we can see in our BPQD solutions there are particles being photo-excited and can relax back down through the emission of photons. This combined with the absorbance data also collected should allow for the generated BPQDs to absorb solar photons and excite electrons. Further experiments will uncover how productive those excited electrons can be.

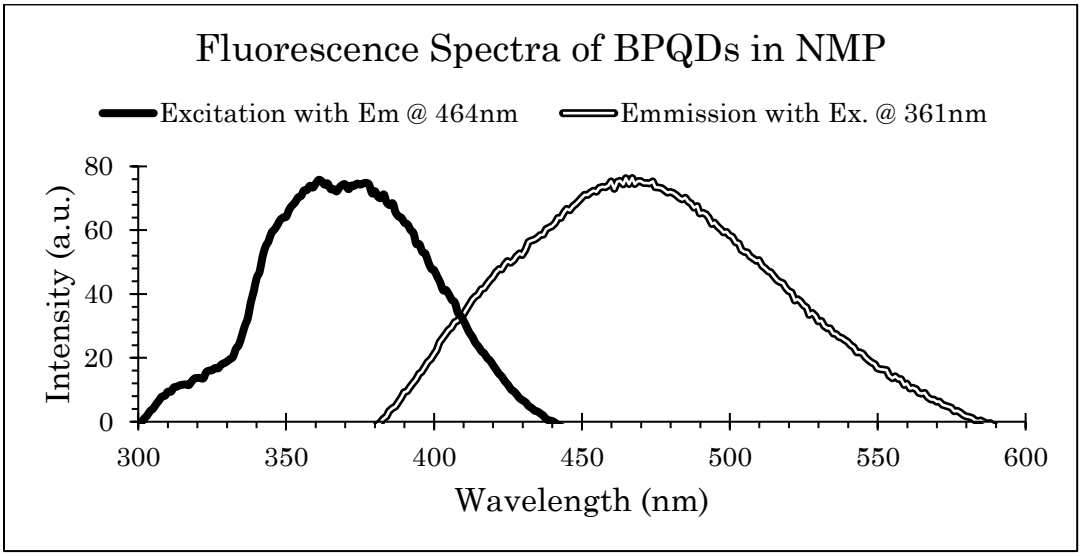

Figure21: Fluorescence spectra of BPQDs in NMP; Excitation profile while scanning for emission @ 464 nm (solid) and emission profile while exciting at 361 nm (hollow).

2.2.2 Methyl viologen as an electron transfer probe

As a way of testing if the generated BPQD samples could transfer excited electrons, a system was devised to utilize methyl viologen as a colorimetric probe.

Methyl viologen (MV^{2+}) is a dication that can be easily reduced to a colored mono or di-radicaloid (Figure 22). When reduced, this species produces prominent peaks in UV-Vis spectra around 398 nm and 605 nm[55] that can lead to confirmation of productive electron transfer to methyl viologen in-situ.

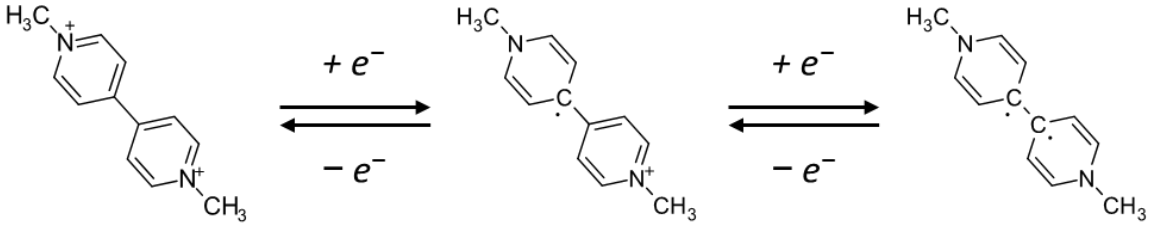

Figure 22: Reduction of methyl viologen dication to colored radicaloid species

The first experiment was performed using 0.50 mL of 0.01 M methyl viologen dichloride solution, 1.50 mL of 0.01 M ascorbic acid (AA), and 0.500 mL of a standard BPQD solution. These portions were combined into a sealed borosilicate glass tube, covered with aluminum foil to protect from ambient light, and sparged with nitrogen for 20 min. 1.0 mL of this solution was then transferred to a sealed nitrogen-filled quartz cuvette. The cuvette was irradiated and stirred for approximately 4.5 h but, no color change was observed. UV-Vis absorbance spectra were obtained before and after irradiation and show no appearance of peaks that could be assigned to reduced methyl viologen radical species.

A different electron donor, ethylenediaminetetraacetic acid (EDTA), was used instead of AA to attempt to determine if this was having an effect. Five solutions were prepared, including controls with no BPQDs and no electron donor (Table 1). These solutions were set up as previously described and irradiated for a total of 1 h. UV-Vis

spectra were obtained before irradiation, after 25 min and after 1 h of irradiation. None of these solutions showed any color changes and no significant peaks were observed in the UV-Vis spectra.

Table 1: Conditions for probing aqueous electron transfer to MV^{2+} using 0.03 mg/mL BPQDs in NMP, 0.033 M aqueous methylviologen dichloride, and 0.2 M aqueous electron donor solutions, and dionized water. Total volume for all solutions was 3.50 mL

X	BP (mL)	BP (mg)	MV^{2+} (mL)	MV^{2+} (mol)	Donor ID	Donor (mL)	Donor (mol)
A	0.50	0.015	1.50	0.000050	AA	1.50	0.00030
B	0.50	0.015	1.50	0.000050	EDTA	1.50	0.00030
C	0.00	0.000	1.50	0.000050	AA	1.50	0.00030
D	0.00	0.000	1.50	0.000050	EDTA	1.50	0.00030
E	0.50	0.015	1.50	0.000050	none	0.00	0.00000

These results may be potentially explained by the instability of BPQDs in water. Dark colored precipitates could be seen in the bottom of the tubes after illumination suggesting BPQDs were either aggregating or decomposing. This led to the exploration of acetonitrile as a suitable replacement solvent. Luckily, the methyl viologen salt being used was soluble in acetonitrile but, the electron donors used so far were not. Therefore, dimethylaniline (DMA) and potassium xanthogenate (KXan) were explored as electron donor candidates. It should be noted that TEOA was also investigated as it is miscible with acetonitrile but, previous work has shown that TEOA can form a colored charge-transfer complex with methyl viologen causing a false positive result.[56]

Acetonitrile solutions were prepared similar to previously discussed aqueous solutions (Table 2). These solutions were irradiated for 1h and a UV-Vis spectrum measured at the same intervals as in previous experiments. Surprisingly, the only

solution that showed any color change and the appearance of new peaks in the UV-Vis spectrum was the control without electron donor.

Table 2: Conditions for probing electron transfer to MV^{2+} using 0.03 mg/mL BPQDs in NMP, 0.033 M methylviologen dichloride in MeCN, and 0.2 M electron donor MeCN solutions, and MeCN. Total volume for all solutions was 3.00 mL

Sample	BP (mL)	MV^{2+} (mol)	Donor ID	Donor (mol)	MeCN (mL)
A	0.50	0.00005	DMA	0.00015	2.5
B	0.50	0.00005	KXan	0.00015	2.5
C	0.00	0.00005	DMA	0.00015	3.0
D	0.00	0.00005	KXan	0.00015	3.0
E	0.50	0.00005	none	0.00000	2.5

This control with no electron donor was repeated with more frequent measurement of UV-Vis spectra to better illustrate the growth of the reduced methyl viologen peaks over time (Figure 23). This result shows that black phosphorus can reduce methyl viologen in acetonitrile but that the choice in electron donors could interfere with productive electron transfer.

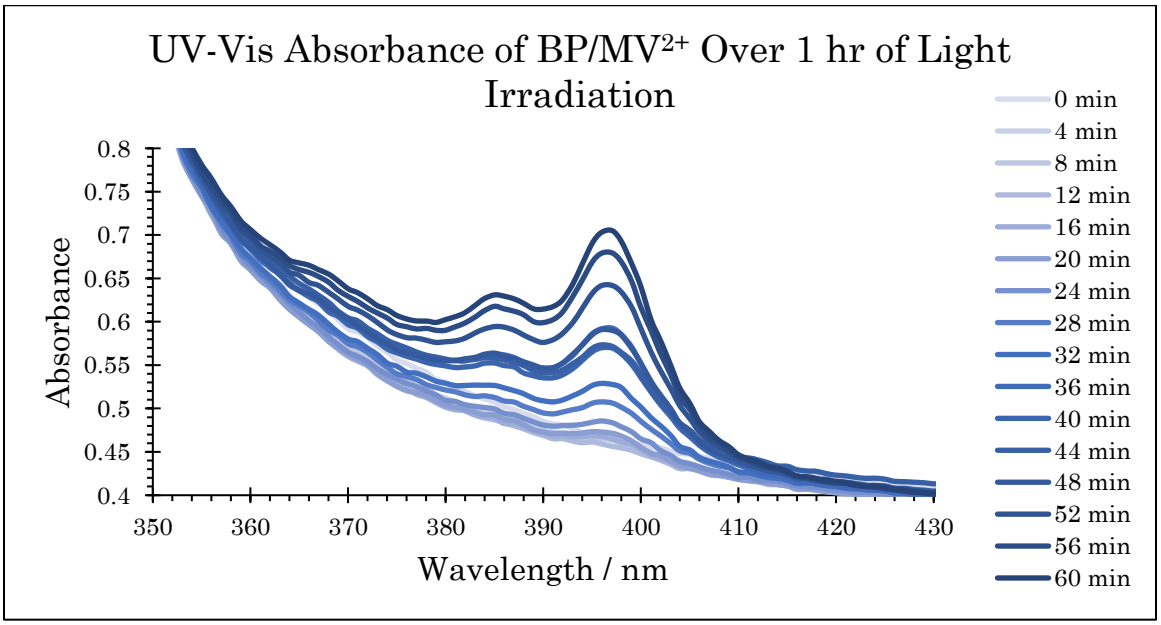

Figure 23: Stacked UV-Vis spectra of irradiated BPQD and MV^{2+} in acetonitrile over time showing an increase for activated methyl viologen.

2.3 Testing Photocatalytic Capabilities of BPQDs

The first photocatalytic systems involving black phosphorus in this work involved using platinum as a co-catalyst. Our proposed system involved using K_2PtCl_6 to be reduced into platinum nanoparticles onto the surface of BPQDS in-situ (Figure 16). This should allow for easier electron transfer between the BPQDs and Pt due to their surface deposition.

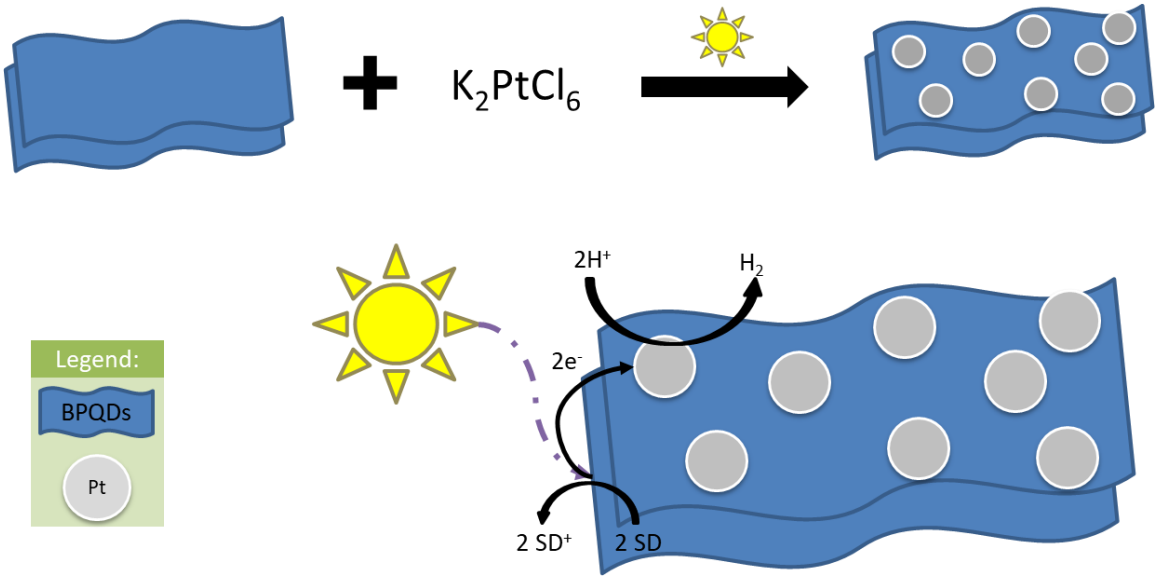

Figure 24: Schematic of photocatalytic generation of H_2 using BPQDs, platinum nanoparticles, and a sacrificial electron donor (SED)

To test the photocatalytic abilities of this type of system 6 solutions using various amounts of a standard BP solution, 0.11 M aqueous K_2PtCl_6, and a 5:1 dimethylformamide (DMF) to triethanolamine (TEOA) solution were combined in separate, sealed borosilicate tubes with stir bars (Table 3). Due to the potential for degradation of BPQDs in water and the need for an electron donor to complete the catalytic cycle a mixed solvent system involving DMF and TEOA was chosen. These

solutions were covered in aluminum foil while being sparged with nitrogen to create an oxygen-free environment during photocatalysis. The solutions were then placed inside a temperature-controlled water bath at 20 °C with a quartz window in front of a solar simulator. After one hour of illumination a headspace analysis was performed via GC-TCD. No hydrogen was observed after 1 h of irradiation, thus the solutions were placed back in front of the solar lamp overnight. After 15 h of light irradiation, no hydrogen was observed in the gas chromatogram.

Table 3: Samples created for photocatalytic production of hydrogen using a 0.11 M aqueous solution of K_2PtCl_6, 0.03 mg/mL BPQD in NMP, and a 5:1 DMF:TEOA solution. Total solution volume for each sample was 3.0 mL.

Sample	BP (mg)	K_2PtCl_6 (mol)	Pt:BP (wt/wt)	DMF:TEOA (mL)
1	0.003	0.00000	0.00E+00	2.9
2	0.006	0.00000	0.00E+00	2.8
3	0.009	0.00000	0.00E+00	2.7
4	0.003	0.00017	1.07E+04	1.4
5	0.006	0.00017	5.36E+03	1.3
6	0.009	0.00017	3.58E+03	1.2

Upon calculating the platinum loading, it was determined that the platinum loading for the samples above was much too high, potentially blocking the penetration of light to the BPQD. Thus, a new set of samples were prepared with a lower Pt loading. BP concentration in standard solution was originally estimated based on starting amount of bulk BP before sonication, which was a gross over-estimation. A target Pt loading of 0.25 % (wt/wt) was chosen but, updated concentration measures show this was overshot. Three samples were prepared like previous photocatalysis experiments (Table 4). Even after 15 h of illumination, none of the samples showed any production of hydrogen by GC headspace analysis.

Table 4: Photocatalysis samples using a lower platinum loading. A 0.11 M aqueous solution of K_2PtCl_6 was combined with a standard, 0.03 mg/mL, BPQD in NMP, and a 5:1 DMF:TEOA solution. Total solution volume for each sample was 3.0 mL.

Sample	BP (mg)	K_2PtCl_6 (mol)	Pt:BP (wt/wt)	DMF:TEOA (mL)
1	0.015	3.63E-06	47.21	2.47
2	0.0225	5.39E-06	46.73	2.2
3	0.03	7.15E-06	46.50	1.93

Various solutions were prepared to compare pre-synthesized citrate-capped platinum nanoparticles to platinum reduced on BPQDs in-situ (Table 5). Colloidal platinum nanoparticles were chosen since we could confirm nanoparticle formation before utilizing them in photocatalytic experiments. A brief description of the synthesis and characterization of the solutions used in this experiment can be found in the Experimental (Section 4.3.8). Several common liquid electron donors were chosen; acetic acid (AcOH), triethanolamine (TEOA), and triethylamine (TEA). Tetrabutylammonium hydrogen sulfate (TBA·HSO_4) was also chosen as an electron donor because it can also act as a proton donor. Excess protons are required to produce hydrogen in the absence of water as a solvent. Aside from this donor, all protons originate from the water in the aqueous platinum solutions used.

Table 5: Conditions for acetonitrile-based hydrogen generation experiments using 0.03 mg/mL BPQDs in NMP, 0.1 M electron donor solutions in acetonitrile, 25 mM aqueous K_2PtCl_6, and 6 mM aqueous Pt@Citrate. All samples also contained 0.25 mL deionized water and were diluted to 5.00 mL using acetonitrile.

#	BP (mg)	Donor ID	Donor (mol)	Catalyst ID	Cat. (mol)	Pt (mg)	Pt:BP (wt/wt)
1	0.015	AcOH	0.00024	Pt@Citrate	6.00E-08	1.17E-02	7.80E-01
2	0.015	AcOH	0.00024	K_2PtCl_6	2.50E-07	2.50E-07	1.67E-05
3	0.015	TEA	0.00024	Pt@Citrate	6.00E-08	1.17E-02	7.80E-01
4	0.015	TEA	0.00024	K_2PtCl_6	2.50E-07	2.50E-07	1.67E-05
5	0.015	TEOA	0.00024	Pt@Citrate	6.00E-08	1.17E-02	7.80E-01
6	0.015	TEOA	0.00024	K_2PtCl_6	2.50E-07	2.50E-07	1.67E-05

Solutions were combined with stir bars in separate borosilicate glass tubes, were sparged with nitrogen for 20 min while covered with aluminum foil to protect against ambient light, and then placed in a temperature-controlled water bath with a quartz window in front of a solar simulator. Solutions were irradiated overnight for a total of 16 h. A headspace gas analysis was performed using a GC-TCD to monitor hydrogen production. None of the chromatograms for these solutions showed evidence of hydrogen production.

To test if the amount of electron donor utilized was sufficient two solutions were prepared with significantly higher ED concentrations (Table 6). The headspace gas analysis for these samples indicated that the increased electron donor concentration led to the production of hydrogen. A calculated 4.3 x 10^{-7} mol of H_2 was produced after 1h of irradiation resulting in an activity of 1.43 x 10^{-2} $\frac{mol\ H_2}{g\ BP\ x\ h}$. This is close to the previously reported activity for BPQDs by the Mathews group, 4 x 10^{-3} $\frac{mol\ H_2}{g\ BP\ x\ h}$.[35]

Table 6: Experimental conditions for electron donor concentration change. Created using 0.03 mg/mL BPQDs in MeCN, neat (1) or 0.1M TEOA in acetonitrile (2), deionized water, and diluted to 5.00 mL using acetonitrile.

Sample	BP (mg)	TEOA (mol)	H_2O (mL)	Total mL
1	0.03	0.02967	0.25	5.00
2	0.03	0.00038	0.25	5.00

Six solutions using previously used electron donors at higher concentrations were prepared (Table 7). Unfortunately, these solutions also did not show any H_2 production based on the headspace gas analysis by GC which was performed after 1 h of irradiation.

Table 7: Experimental conditions for acetonitrile-based hydrogen generation experiments using 0.03 mg/mL BPQDs in NMP, 2.08 M electron donor solutions in acetonitrile, 25 mM aqueous K_2PtCl_6, and 6 mM aqueous Pt@Citrate. All samples also contained 0.25 mL deionized water and were diluted to 5.00 mL using acetonitrile.

#	BP (mg)	Donor ID	Donor (mol)	Catalyst ID	Cat. (mol)	Pt (mg)	Pt:BP (wt/wt)
1	0.015	AcOH	0.005	Pt@Citrate	6.00E-08	1.17E-02	7.80E-01
2	0.015	AcOH	0.005	K_2PtCl_6	2.50E-07	2.50E-07	1.67E-05
3	0.015	TEA	0.005	Pt@Citrate	6.00E-08	1.17E-02	7.80E-01
4	0.015	TEA	0.005	K_2PtCl_6	2.50E-07	2.50E-07	1.67E-05
5	0.015	TEOA	0.005	Pt@Citrate	6.00E-08	1.17E-02	7.80E-01
6	0.015	TEOA	0.005	K_2PtCl_6	2.50E-07	2.50E-07	1.67E-05

3 CONCLUSIONS & FUTURE WORK

3.1 SUMMARY OF FINDINGS

The synthesis of BPQDs through liquid exfoliation of bulk BP crystals was attempted and generated samples were characterized through SEM, DLS, and AFM. Images generated through SEM were useful for seeing many particles at once with decent resolution until particles under 200 nm were seen. DLS results began disagreeing with other characterizations results. This was likely due to the polydisperse, irregularly shaped, photoactive BP particles generated. AFM was a powerful imaging technique that allowed for the measurement of the heights of generated particles. Due to the low power level of the utilized sonication devices sonication times needed to produce BPQDs of < 100 nm far exceeded those found in the literature.

The photo-physical properties of BPQDs were explored using UV-Vis and fluorescence spectroscopy. BPQDs in NMP show a broad absorbance signal that extends deeply into the visible region of light. Fluorescence spectroscopy studies reveal that BPQDs are capable of absorbing photons to excite electrons that will relax back to a ground state if given enough time.

Electron transfer experiments were performed using a methyl viologen di-cation as a colorimetric probe. In these experiments BPQDs were combined with MV^{2+} and/or a series of electron donors, illuminated, and UV-vis spectroscopy was used to scan for MV radicaloids as an indication of electron transfer. The only solution to

show photo-chemical reduction of MV^{2+} was a solution created using only BPQDs and MV^{2+} in MeCN. This result showed that while the choice in sacrificial electron could be fatal, BPQDs were capable of photo-reducing MV^{2+}.

The capabilities of BPQDs to photocatalytically produce hydrogen gas was explored by creating solutions using differing combinations of BPQDs, electron donors, platinum based co-catalysts, and solvents. Dark colored precipitates, believed to be BPQDs or decomposition products, were observed for aqueous systems. Platinum was introduced into the system by either photochemically reducing K_2PtCl_6 to form platinum nanoparticles on the surface of BPQDs or by adding pre-synthesized citrate capped platinum nanoparticles to the photocatalysis solutions. Electron donor concentrations were found to be very important to the photo-generation of hydrogen gas in these systems. Hydrogen gas production was only observed for an acetonitrile system containing BPQDs, no co-catalyst, and TEOA as a sacrificial donor. A calculated 4.3×10^{-7} mol of H_2 was produced after 1h of irradiation resulting in an activity of $1.43 \times 10^{-2} \frac{mol\ H_2}{g\ BP\ x\ h}$. This is close to the previously reported activity for BPQDs by the Mathews group, $4 \times 10^{-3} \frac{mol\ H_2}{g\ BP\ x\ h}$ under similar conditions.[35]

Since none of the platinum containing systems produced hydrogen, there must be some unfavorable interactions going on. In the case of the in-situ reduced K_2PtCl_6 it is unknown where the platinum deposits are forming, if they are forming at all. It is possible that not enough illumination time was given to allow the photo-reduction to occur completely, meaning all excited electrons generated were being fed into forming

deposits and none were able to go towards hydrogen production. It is also possible that the platinum deposits could be blocking active sites on the surface of BPQDs, shutting down their catalytic abilities. There could also be structural or electronic interference in the BPQDs after platinum has deposited onto the surface.

Most of these scenarios would be avoided in the utilization of citrate-capped platinum nanoparticles. Since the particles are generated and characterized before addition, it is known that have indeed been formed. It is not known however, how the Pt@Citrate nanoparticles are interacting with the BPQDs.

3.2 FUTURE WORK

To further understand what is going on in the platinum based systems a few experiments could be performed. Combining BPQDs with K_2PtCl_6, illuminating, and then observing, via SEM, a dropcasted sample of that solution could provide insight on how the two materials are interacting. SEM with an EDX detector could differentiate BPQDs and Pt nanoparticles based on their elemental make-up due to the large difference in their atomic masses. This could be used to see if platinum is forming deposits onto BP at all, and what size those deposits may be. This method can also be used to determine illumination time required to form deposits in the first place. Utilizing H_2PtCl_6 in place of K_2PtCl_6 in the photocatalytic experiments attempted in this work might also prove fruitful. As H_2PtCl_6 is more acidic, the change in pH of the system could affect the photocatalytic abilities.

Alternative co-catalysts should be utilized in the presence of BPQDs for the photogeneration of hydrogen. Tian and colleagues were able to synthesize a BP-CoP hybrid material through a solvothermal process[45] but, there material was much larger than the BPQDs generated in this work. A cobalt precursor salt, such as $Co(NO_3)_2$, could be used to reduce cobalt and form deposits onto BPQDs much like the attempted K_2PtCl_6 experiments. This sort of system could have all the successes of the BP-CoP hybrid material with the added advantages of BPQDs; larger surface area to mass ratio and improved visible light absorption.

Lastly, homogenous systems using molecular catalysts instead of the proposed heterogenous once, could be more successful. There are many well-researched, effective catalysts that could be chosen.[57] There will just have to be care in choosing a catalyst whose band position lines up well with BPQDs. Band positions for the materials used in this work were not able to be measured but, previous work estimates BPQDs conduction band could around −1.0 V vs. SHE.[42]

4 EXPERIMENTAL METHODS & MATERIALS

4.1 MATERIALS

All black phosphorus crystals used in these experiments were purchased from Smart Elements. All other chemical materials were purchased from Fisher Scientific. All black phosphorus crystals, NMP, BPQD samples, and de-gassed solvents were stored and handled in a nitrogen filled glovebox.

4.2 BPQD SYNTHESIS AND ISOLATION

4.2.1 General Method for Synthesizing BPQDs via Sonication

In a nitrogen-filled glove box, approximately 10 mg of bulk Black Phosphorus was weighed out. Using an agate mortar and pestle the BP was ground with a few drops of NMP (N-methyl-pyrrolidone) and then added to a 20 mL vial. Following, an additional 10 mL of NMP was added to the vial. Using a Hielscher UP100H ultrasonic processor with an MS7 sonotrode, referred to as a probe sonicator herein, the sample is sonicated for 3 h. Once removed the hot sample was capped and allowed to cool. The sample vial was protected from ambient conditions by the addition of Teflon tape around the cap. The sample was then placed in an ice-cooled Branson 2510 Ultrasonic Cleaner, referred to as a bath sonicator herein, for 10 hours. Since this process causes the bath to increase in temperature ice was continually added to keep the sample from overheating. After the sonication was completed the sample was brought back into the glovebox for storage.

The sonicated sample was then added to a centrifuge tube made of FEP (fluorinated ethylene propylene) and weighed out to prepare a counter-balanced tube of water. The sample was centrifuged at 9000 rpm for 15 minutes and the supernatant was kept in a new vial.

If the dots need to be placed in a new solvent, for imaging prep as an example, the sample is centrifuged at 11382 rpm for another 30 minutes and the dots were found in the pellet were re-dispersed in a new solvent after the supernatant has been removed. Additional washes with the new solvent can be performed using the same spin conditions.

4.2.2 Synthesizing CAA1-007

In a nitrogen-filled and solvent-free glove box, 0.015g of bulk BP crystals were weighed out and added to a small vial. This vial was then transferred to a "wet" nitrogen-filled glovebox and 10mL of NMP was added to the vial and sonicated via an ultrasonic probe for three hours. The resulting suspension was a silver-grey color with a noticeable sheen when stirred. The vial was then sealed tightly using Teflon tape and a cap and taken out of the glovebox for bath sonication. The sample was sonicated for 10 hours. To crash out the larger dots, the sample was centrifuged at 9000 rpm for 15 minutes. The supernatant was carefully removed from the crashed-out BP and sealed in a new vial.

4.2.3 Synthesizing CAA1-009

In a nitrogen-filled and solvent-free glove box, 0.013g of bulk BP crystals were weighed out and added to a small vial. This vial was then transferred to a "wet"

nitrogen-filled glovebox and 10mL of NMP was added to the vial and sonicated via an ultrasonic probe for three hours. The resulting suspension was a silver-grey color with a noticeable sheen when stirred. In order to crash out the larger dots, the sample was centrifuged at 9000 rpm for 15 minutes. The supernatant was carefully removed from the crashed-out BP and sealed in a new vial

4.2.4 Synthesizing CAA1-011

This procedure is adapted from literature.[41] In a nitrogen-filled and solvent-free glovebox, 0.025 g of bulk BP crystals were weighed out and transferred to an amber vial. 250 mL of DMSO was measured out and added to a glass kitchen blender along with the BP crystals. The blender was turned on to its highest setting: "blend icy drink". The mixture was blended for 40 minutes before turning the blender off. The blender was hot to touch, and the plastic cap was noticeably damaged. The mixed sample was added to two 125mL bottles for storage. To crash out the larger particles, the samples were centrifuged at 9000 rpm for 15 minutes and only the top 50% of the solution was kept.

4.2.5 Synthesizing CAA1-014

In a nitrogen-filled and solvent-free glovebox, 0.030 g of bulk BP crystals were weighed out and transferred to an amber vial. 100 mL of DMSO was measured out and added to a glass kitchen blender along with the BP crystals. The blender was turned on to its highest setting: "blend icy drink". The mixture was blended for 40 min before turning the blender off. The mixed sample was added to a 125 mL bottles

for storage. To crash out the larger particles, the samples were centrifuged at 9000 rpm for 15 min and only the top 50% of the solution was kept.

4.2.6 An Attempt at PEG Passivation (CAA1-015)

5 mL from CAA1-014 was added to a centrifuge tube and spun at 11,832 rpm for 30 min to crash out all the BP. 1 mg of the crashed-out material was added to 5 mg of PEG (200N) and 10mL of IPA and was sonicated via ultrasonic bath for 30 min. The sample was then allowed to stir for 4 h. The resulting mixture was centrifuged at 11,832 rpm for 30 min. The supernatant was carefully removed, and the crashed-out material was added to 10 mL of IPA.

4.2.7 Synthesizing CAA1-016

In a nitrogen-filled and solvent-free glove box, 0.010 g of bulk BP crystals were weighed out and added to a small vial. This vial was then transferred to a "wet" nitrogen-filled glovebox and 10 mL of NMP was added to the vial and sonicated via an ultrasonic probe for 5 h. The resulting suspension was a silver-grey color with a noticeable sheen when stirred. The vial was then sealed tightly using Teflon tape and a cap and taken out of the glovebox for bath sonication. The sample was sonicated for 10 h. To crash out the larger dots, the sample was centrifuged at 9000 rpm for 15 min. The supernatant was carefully removed from the crashed-out BP and sealed in a new vial.

4.2.8 Synthesizing CAA1-023 (extended sonication time)

In a nitrogen-filled and solvent-free glove box, 0.010 g of bulk BP crystals were weighed out and added to a small vial. This vial was then transferred to a "wet"

nitrogen-filled glovebox and 10 mL of NMP was added to the vial and sonicated via an ultrasonic probe for 10 h. The resulting suspension was a silver-grey color with a noticeable sheen when stirred. The vial was then sealed tightly using Teflon tape and a cap and taken out of the glovebox for bath sonication. The sample was sonicated for 16 h. To crash out the larger dots, the sample was centrifuged at 9000 rpm for 15 min. The supernatant was carefully removed from the crashed-out BP and sealed in a new vial.

4.2.9 Synthesizing CAA1-027 (Higher concentration of BP)

In a nitrogen-filled and solvent-free glove box, 0.050 g of bulk BP crystals were weighed out and added to a small vial. This vial was then transferred to a "wet" nitrogen-filled glovebox and 10 mL of NMP was added to the vial and sonicated via an ultrasonic probe for 10 h. The resulting suspension was a silver-grey color with a noticeable sheen when stirred. The vial was then sealed tightly using Teflon tape and a cap and taken out of the glovebox for bath sonication. The sample was sonicated for 16 h. To crash out the larger dots, the sample was centrifuged at 9000 rpm for 15 min. The supernatant was carefully removed from the crashed-out BP and sealed in a new vial.

4.3 Photocatalysis & Electron Transfer Probe Experiments

4.3.1 General Notes Regarding BPQD Solutions and Oxygen Removal Strategies:

All BPQD solutions used during photocatalysis and electron transfer probe experiments were made using the same conditions. 0.030 g of bulk BP crystals were grinded and sonicated in 10 mL of NMP and isolated via centrifugation as described earlier.

All other solutions mentioned in this section have has some form of oxygen removal considered. All solutions were bubbled with nitrogen for more than 20 min before using them in any experiments to help remove any oxygen that may be present. All BPQD and NMP solutions are stored in a nitrogen filled glovebox fitted with a copper catalyst for oxygen removal. Organic solutions are degassed through a freeze-pump-thaw method while aqueous solutions are sonicated under reduced pressure before being introduced into the glovebox for storage.

4.3.2 Scanning for Photogeneration of Hydrogen Gas: Pt Co-catalyst, TEOA, and DMF

Using a 0.11 M solution of K_2PtCl_6 in water, a 5:1 (v/v) DMF:TEOA solution, and a standard BPQD solution, six solutions of varying BPQD concentration and platinum loading were created (Table 8)

Table 8: Samples created for photocatalytic production of hydrogen using a 0.11 M aqueous solution of K_2PtCl_6, 0.03 mg/mL BPQD in NMP, and a 5:1 DMF:TEOA solution. Total solution volume for each sample was 3.0 mL.

#	BP (mL)	BP (mg)	K_2PtCl_6 (mL)	K_2PtCl_6 (mol)	Pt (mg)	Pt:BP (wt/wt)	DMF:TEOA (mL)
1	0.1	0.003	0	0.00000	0.000	0.00E+00	2.9
2	0.2	0.006	0	0.00000	0.000	0.00E+00	2.8
3	0.3	0.009	0	0.00000	0.000	0.00E+00	2.7
4	0.1	0.003	1.5	0.00017	32.189	1.07E+04	1.4
5	0.2	0.006	1.5	0.00017	32.189	5.36E+03	1.3
6	0.3	0.009	1.5	0.00017	32.189	3.58E+03	1.2

4.3.3 Scanning for photocatalysis using a lower platinum loading

Using a 0.11 M K_2PtCl_6 aqueous solution, a 5:1 DMF:TEOA solution, and a standard BPQD solution three new solutions were prepared (Table 9)

Table 9: Photocatalysis samples using a lower platinum loading. A 0.11 M aqueous solution of K_2PtCl_6 was combined with a standard, 0.03 mg/mL, BPQD in NMP, and a 5:1 DMF:TEOA solution. Total solution volume for each sample was 3.0 mL.

#	BP (mL)	BP (mg)	K_2PtCl_6 (mL)	K_2PtCl_6 (mol)	Pt (mg)	Pt:BP (wt/wt)	DMF:TEOA (mL)
1	0.50	0.0150	0.033	3.63E-06	0.708	47.21	2.47
2	0.75	0.0225	0.049	5.39E-06	1.052	46.73	2.2
3	1.00	0.0300	0.065	7.15E-06	1.395	46.50	1.93

4.3.4 Activation of Aqueous Methyl Viologen via BPQD-mediated photochemical reduction

0.0130 g of methyl viologen (MV^{2+}) was added to a 5mL volumetric flask and diluted to the line with deionized water to create a 0.01 M solution. 0.0090 g of

ascorbic acid was added to a separate 5mL volumetric flask and diluted to the line with deionized water to make a 0.01 M solution. An 8 mL borosilicate tube and septum were brought into the glovebox and 0.500 mL of a standard BPQD solution was added and the tube was subsequently sealed with the septum. Aluminum foil was wrapped the tube upon exiting the glovebox. 0.50 mL of the methyl viologen solution and 1.50 mL of the ascorbic acid solution were added to the sealed tube using a needle and syringe. Using a needle attached to a Schlenk line and a vent needle, nitrogen was bubbled through the solution for 20 min. Using a syringe and needle approximately 1 mL of the solution was transferred to a septum-sealed, nitrogen-purged, quartz cuvette. The cuvette was placed in line of a beam of solar-simulated light for approximately 3 h. A UV-Vis absorbance spectrum was obtained before and after the illumination period.

4.3.5 Activation of Methyl Viologen via BPQD-mediated photochemical reduction in Acetonitrile in the presence of TEOA

0.0130 g of methyl viologen was added to a 5 mL volumetric flask and diluted to the line with acetonitrile to create a 0.01 M solution. A 5 mL 1:5 (v/v) TEOA:MeCN solution was also prepared. An 8 mL borosilicate tube and septum were brought into the glovebox and 0.500 mL of a standard BPQD solution was added and the tube was subsequently sealed with the septum. Aluminum foil was wrapped the tube upon exiting the glovebox. 0.50 mL of the methyl viologen solution and 1.50 mL of the TEOA:MeCN solution were added to the sealed tube using a needle and syringe. Using a needle attached to a Schlenk line and a vent needle, nitrogen was bubbled

through the solution for 20 min. Using a syringe and needle approximately 1 mL of the solution was transferred to a septum-sealed, nitrogen-purged, quartz cuvette. A blue tint to the solution was noticed at this point. The cuvette was then placed in line of a beam of solar-simulated light for approximately 1 h and the blue color became much more prevalent. A UV-Vis absorbance spectrum was obtained before and after the illumination period.

4.3.6 Activation of Methyl Viologen via BPQD-mediated photochemical reduction in Acetonitrile in the presence of various electron donors

Five solutions were created, similarly to previous methyl viologen experiments (Table 10). The solutions were placed into separate 8 mL borosilicate tubes, covered with aluminum foil, and sparged with nitrogen for 20 min. The solutions were then placed in front of a solar light simulator for an hour and UV-Vis Spectra were obtained for each before illumination, after 25 min of illumination, and after an hour of illumination.

Table 10: Samples generated for methyl viologen probe experiment in MeCN using 0.03 mg/mL BPQDs in NMP, 0.033 M methyl viologen dichloride in MeCN, liquid DMA, and solid KXan. Ssamples were diluted to 3.0 mL using MeCN.

X	BP (mL)	BP (mg)	MV^{2+} (mol)	Donor ID	Donor (mol)	MeCN (mL)
A	0.50	0.0015	0.00005	DMA	0.00015	2.5
B	0.50	0.0015	0.00005	KXan	0.00015	2.5
C	0.00	0.0000	0.00005	DMA	0.00015	3.0
D	0.00	0.0000	0.00005	KXan	0.00015	3.0
E	0.50	0.0015	0.00005	none	0.00000	2.5

4.3.7 Activation of Methyl Viologen via BPQD-mediated photochemical reduction in Water in the presence of various electron donors

Five solutions were created, according to the table below, similarly to previous methyl viologen experiments. A 0.033 M solution of MV^{2+} and a 0.2 M solution for each donor were prepared. The sample solutions were placed into separate 8 mL borosilicate tubes, covered with aluminum foil, and sparged with nitrogen for 20 min. The solutions were then placed in front of a solar light simulator for an hour and UV-vis Spectra were obtained for each before illumination, after 25 min of illumination, and after an hour of illumination.

Table 11: Conditions for probing aqueous electron transfer to MV^{2+} using 0.03 mg/mL BPQDs in NMP, 0.033 M aqueous methylviologen dichloride, and 0.2 M aqueous electron donor solutions, and dionized water. Total volume for all solutions was 3.50 mL

X	BP (mL)	MV^{2+} (mL)	MV^{2+} (mol)	Donor ID	Donor (mL)	Donor (mol)
A	0.50	1.50	0.00005	AA	1.50	0.00030
B	0.50	1.50	0.00005	EDTA	1.50	0.00030
C	0.00	1.50	0.00005	AA	1.50	0.00030
D	0.00	1.50	0.00005	EDTA	1.50	0.00030
E	0.50	1.50	0.00005	none	0.00	0.00000

4.3.8 Photogeneration of Hydrogen using BPQDs as a photosensitizer, platinum as a co-catalyst, and various electron donors in acetonitrile

A 0.1 M solution of electron donors; acetic acid (AcOH), $TBAHSO_4$, triethanolamine (TEOA), and triethylamine (TEA), were prepared in acetonitrile. Citrate capped platinum nanoparticles (Pt@Citrate) were synthesized according to literature.[58] 1.0 mL of an aqueous 16 mM H_2PtCl_6 was allowed to hydrolyze for 3 hours before being combined with 1.0 mL of an aqueous 40 mM trisodium citrate solution. This combination was diluted to 40 mL with water and vigorously stirred

for 1 h. 0.200 mL of a freshly prepared 50 mM $NaBH_4$ solution was added dropwise to the mixture. The solution changed from colorless to a brownish yellow indicating the formation of nanoparticles. To characterize these nanoparticles a TEM image was generated by dropcasting the described solution onto a silicon chip. (Figure 25)

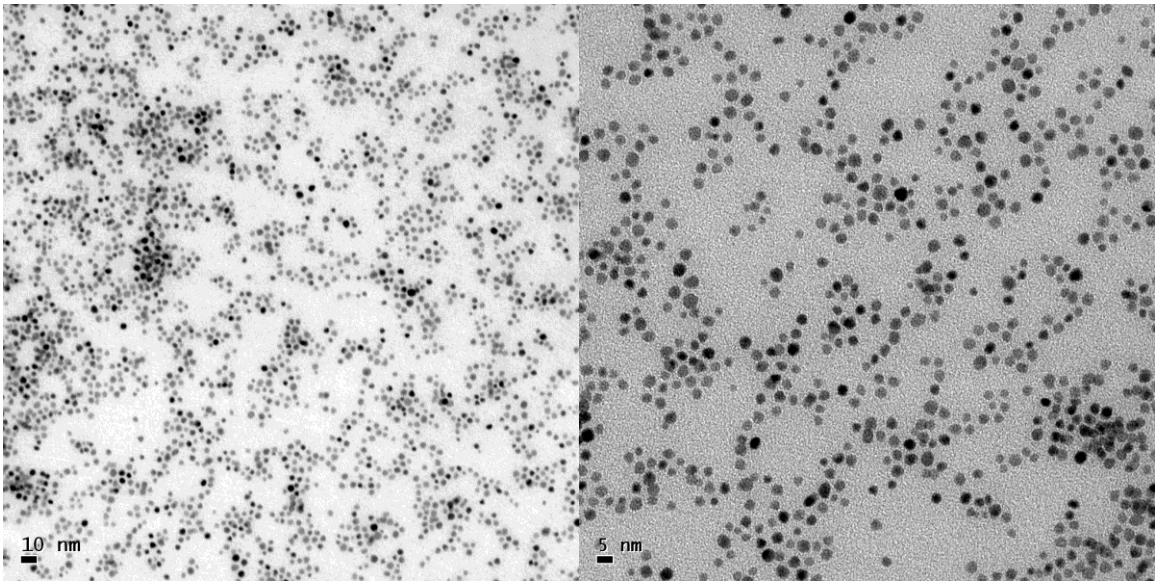

Figure 25: TEM images of synthesized citrate capped platinum nanoparticles

Solutions were combined (Table 12) in separate 8 mL borosilicate tubes, sparged with nitrogen for 20 min while covered with aluminum foil, and then placed in a temperature-controlled water bath in line of a solar light simulator. Solutions were illuminated for a total of 16 h. A headspace analysis was performed using a GC to scan for hydrogen production.

Table 12: Experimental conditions for acetonitrile-based hydrogen generation experiments using 0.03 mg/mL BPQDs in NMP, 0.1 M electron donor solutions in acetonitrile, 25 mM aqueous K_2PtCl_6, and 6 mM aqueous Pt@Citrate. All samples also contained 0.25 mL deionized water and were diluted to 5.00 mL using acetonitrile.

#	BP (mL)	BP (mg)	Donor ID	Donor (mol)	Catalyst ID	Cat. (mol)	Pt (mg)	Pt:BP (wt/wt)
1	0.50	0.015	AcOH	0.00024	Pt@Citrate	6.00E-07	0.117	7.80
2	0.50	0.015	AcOH	0.00024	K_2PtCl_6	2.50E-07	0.049	3.25
3	0.50	0.015	$TBAHSO_4$	0.00024	Pt@Citrate	6.00E-07	0.117	7.80
4	0.50	0.015	$TBAHSO_4$	0.00024	K_2PtCl_6	2.50E-07	0.049	3.25
5	0.50	0.015	TEOA	0.00024	Pt@Citrate	6.00E-07	0.117	7.80
6	0.50	0.015	TEA	0.00024	Pt@Citrate	6.00E-07	0.117	7.80

4.3.9 Testing for a different electron donor concentration to generate hydrogen gas using BPQDs as a photocatalyst in acetonitrile

3 mL BPQDs in NMP were centrifuged at 12000 rpm for 30 min. The top 90% of the solution was removed and the bottom 10% of the solution and the resulting pellet were added to 3 mL of acetonitrile. This new solution was sonicated for 5 minutes to allow the BPQDs to be suspended in the acetonitrile. Two solutions were created in 8 mL borosilicate tubes using the new BPQD-MeCN solution and TEOA, either pure or a 0.1 M solution, according to the table on the next page. These two solutions were sparged with nitrogen for 20 min while covered with aluminum foil, and then placed in a temperature-controlled water bath in front of a solar light simulator. After an hour of illumination, a head space analysis was performed via GC outfitted with a TCD for hydrogen detection.

Table 13: Experimental conditions for electron donor concentration change. Created using 0.03 mg/mL BPQDs in MeCN, neat TEOA (1) or 0.1M TEOA in acetonitrile (2), deionized water, and then diluted to 5.00 mL using acetonitrile.

#	BP (mL)	BP (mg)	TEOA (mol)	H_2O (mL)	Total mL
1	1.00	0.030	0.02967	0.25	5.00
2	1.00	0.030	0.00038	0.25	5.00

4.3.10 Updating BPQD-Pt photocatalysis systems to a higher electron donor concentration

Six solutions were created according to the following table. Each solution was sparged with nitrogen for 20 min while covered in aluminum foil, before being place into a temperature-controlled water bath in front of a solar light simulator. After 1 h of illumination a head space analysis was performed using a GC outfitted with a TCD for hydrogen detection.

Table 14: Experimental conditions for acetonitrile-based hydrogen generation experiments using 0.03 mg/mL BPQDs in NMP, 2.08 M electron donor solutions in acetonitrile, 25 mM aqueous K_2PtCl_6, and 6 mM aqueous Pt@Citrate. All samples also contained 0.25 mL deionized water and were diluted to 5.00 mL using acetonitrile.

#	BP (mg)	Donor ID	Donor (mol)	Catalyst ID	Cat. (mol)	Pt (mg)	Pt:BP (wt/wt)
1	0.015	AcOH	0.005	Pt@Citrate	6.00E-08	1.17E-02	7.80E-01
2	0.015	AcOH	0.005	K_2PtCl_6	2.50E-07	2.50E-07	1.67E-05
3	0.015	TEA	0.005	Pt@Citrate	6.00E-08	1.17E-02	7.80E-01
4	0.015	TEA	0.005	K_2PtCl_6	2.50E-07	2.50E-07	1.67E-05
5	0.015	TEOA	0.005	Pt@Citrate	6.00E-08	1.17E-02	7.80E-01
6	0.015	TEOA	0.005	K_2PtCl_6	2.50E-07	2.50E-07	1.67E-05

4.4 CHARACTERIZATION METHODS

4.4.1 SEM / AFM Sample Prep Methodology

Imaging requires the sample to be drop-cast onto a silicon wafer and therefore requires a bit of manipulation. Solvents like NMP and DMSO are tricky to work with because of their high viscosity and low-volatility. These qualities lead to long evaporation times. To avoid this, it is common to transfer the desired materials into a less viscous and more volatile solvent like IPA. To perform this solvent switch samples in NMP/DMSO are centrifuged at 11,382 rpm for 30 minutes. The supernatant is removed, and the crashed-out particles are dispersed into IPA. The new mixture is then centrifuged again, the solvent removed, and re-dispersed in fresh IPA. This is done another time for a total of three washes, to remove as much of the original solvent as possible.

5 LIST OF REFERENCES

(1) U.S. Energy Information Administration. Energy Explained, Your Guide To Understanding Energy http://www.eia.gov/energyexplained/index.cfm (accessed Jun 1, 2017).

(2) Administration, U. S. E. I. *Annual Energy Outlook 2018 with Projections to 2050*; 2018; Vol. 44.

(3) California Independent System Operator. California ISO Fast Facts http://www.caiso.com/Documents/FlexibleResourcesHelpRenewables_FastFacts.pdf.

(4) Abraham, K. M. Prospects and Limits of Energy Storage in Batteries. *J. Phys. Chem. Lett.* **2015**, *6*, 830–844.

(5) Zhou, H.; Yan, R.; Zhang, D.; Fan, T. Challenges and Perspectives in Designing Artificial Photosynthetic Systems. *Chem. - A Eur. J.* **2016**, *22*, 9870–9885.

(6) Heeger, A. Solar Fuels and Artificial Photosynthesis. **2012**, 1–26.

(7) Bagher, A. M.; Vahid, M.; Mohsen, M. Geothermal Energy. *J. Eng. Technol. Res.* **2014**, *6*, 146–150.

(8) Atkinson, A.; Barnett, S.; Gorte, R. J.; Irvine, J. T. S.; McEvoy, A. J.; Mogensen, M.; Singhal, S. C.; Vohs, J. Advanced Anodes for High-Temperature Fuel Cells. *Nat. Mater.* **2004**, *3*, 17–27.

(9) Nørskov, J. K.; Rossmeisl, J.; Logadottir, A.; Lindqvist, L.; Kitchin, J. R.; Bligaard, T.; Jónsson, H. Origin of the Overpotential for Oxygen Reduction at a Fuel-Cell Cathode. *J. Phys. Chem. B* **2004**, *108*, 17886–17892.

(10) Plunkett Research. *Plunkett's Automobile Industry Almanac*, 2010 ed.; Plunkett Research: Houston, TX, 2010.

(11) Wipke, K.; Sprik, S.; Kurtz, J.; Ramsden, T.; Ainscough, C.; Saur, G. *Controlled Hydrogen Fleet and Infrastructure Analysis*; Washington, DC, 2011.

(12) Culver, M. Global Hydrogen Fuel Cell Electric Vehicle Market Buoyed as OEMs Will Launch 17 Vehicle Models by 2027, IHS Says http://press.ihs.com/press-release/automotive/global-hydrogen-fuel-cell-electric-vehicle-market-buoyed-oems-will-launch-1.

(13) Sharaf, O. Z.; Orhan, M. F. An Overview of Fuel Cell Technology: Fundamentals and Applications. *Renew. Sustain. Energy Rev.* **2014**, *32*, 810–853.

(14) Miesslar, G.; Fischer, P.; Tarr, D. *Inorganic Chemistry*, 5th ed.; Jaworski, A., Ed.; Pearson: Upper Saddle River, NJ, 1923; Vol. 124.

(15) Office, F. C. T. Hydrogen Production: Natural Gas Reforming http://energy.gov/eere/fuelcells/hydrogen-production-natural-gas-reforming (accessed Jun 11, 2018).

(16) Lewis, N. S.; Nocera, D. G. Powering the Planet: Chemical Challenges in Solar Energy Utilization. *Proc. Natl. Acad. Sci.* **2006**, *103*, 15729–15735.

(17) Mazloomi, K.; Gomes, C. Hydrogen as an Energy Carrier: Prospects and Challenges. *Renew. Sustain. Energy Rev.* **2012**, *16*, 3024–3033.

(18) Lewis, N. S.; Nocera, D. G. Powering the Planet: Chemical Challenges in Solar Energy Utilization. *Proc. Natl. Acad. Sci.* **2006**, *103*, 15729–15735.

(19) Morris, A. J.; Meyer, G. J.; Fujita, E. Molecular Approaches to the Photocatalytic Reduction of Carbon Dioxide for Solar Fuels. *Acc. Chem. Res.* **2009**, *42*, 1983–1994.

(20) Willkomm, J.; Orchard, K. L.; Reynal, A.; Pastor, E.; Durrant, J. R.; Reisner, E. Dye-Sensitised Semiconductors Modified with Molecular Catalysts for Light-Driven H2production. *Chem. Soc. Rev.* **2016**, *45*, 9–23.

(21) Lakadamyali, F.; Kato, M.; Reisner, E. Colloidal Metal Oxide Particles Loaded with Synthetic Catalysts for Solar H 2 Production. *Faraday Discuss.* **2012**, *155*, 191–205.

(22) Hagfeldt, A.; Boschloo, G.; Sun, L.; Kloo, L.; Pettersson, H. Dye-Sensitized Solar

Cells. *Chem. Rev.* **2010**, *110*, 6595–6663.

(23) Narayan, M. R. Review: Dye Sensitized Solar Cells Based on Natural Photosensitizers. *Renew. Sustain. Energy Rev.* **2012**, *16*, 208–215.

(24) Esswein, A. J.; Nocera, D. G. Hydrogen Production by Molecular Photocatalysis. *Chem. Rev.* **2007**, *107*, 4022–4047.

(25) Hisatomi, T.; Kubota, J.; Domen, K. Recent Advances in Semiconductors for Photocatalytic and Photoelectrochemical Water Splitting. *Chem. Soc. Rev.* **2014**, *43*, 7520–7535.

(26) Moniz, S. J. A.; Shevlin, S. A.; Martin, D. J.; Guo, Z. X.; Tang, J. Visible-Light Driven Heterojunction Photocatalysts for Water Splitting-a Critical Review. *Energy Environ. Sci.* **2015**, *8*, 731–759.

(27) Reynal, A.; Palomares, E. Ruthenium Polypyridyl Sensitisers in Dye Solar Cells Based on Mesoporous TiO_2. *Eur. J. Inorg. Chem.* **2011**, No. 29, 4509–4526.

(28) Sabatini, R. P.; Eckenhoff, W. T.; Orchard, A.; Liwosz, K. R.; Detty, M. R.; Watson, D. F.; McCamant, D. W.; Eisenberg, R. From Seconds to Femtoseconds: Solar Hydrogen Production and Transient Absorption of Chalcogenorhodamine Dyes. *J. Am. Chem. Soc.* **2014**, *136*, 7740–7750.

(29) Akinwande, D.; Petrone, N.; Hone, J. Two-Dimensional Flexible Nanoelectronics. *Nat. Commun.* **2014**, *5*, 1–12.

(30) askIITians. Phosphorus Allotropic Forms https://www.askiitians.com/iit-jee-s-and-p-block-elements/phosphorus-allotropic-forms/.

(31) Bridgman, P. W. Two New Modifications of Phosphorus. *J. Am. Chem. Soc.* **1914**, *36*, 1344–1363.

(32) Ling, X.; Wang, H.; Huang, S.; Xia, F.; Dresselhaus, M. S. The Renaissance of Black Phosphorus. *Proc. Natl. Acad. Sci.* **2015**, *112*, 4523–4530.

(33) Bhimanapati, G. R.; Lin, Z.; Meunier, V.; Jung, Y.; Cha, J.; Das, S.; Xiao, D.; Son, Y.; Strano, M. S.; Cooper, V. R.; et al. Recent Advances in Two-Dimensional

Materials beyond Graphene. *ACS Nano*. 2015, pp 11509–11539.

(34) Liu, H.; Neal, A. T.; Zhu, Z.; Luo, Z.; Xu, X.; Tománek, D.; Ye, P. D. Phosphorene: An Unexplored 2D Semiconductor with a High Hole Mobility. *ACS Nano* **2014**, *8*, 4033–4041.

(35) Du, Y.; Ouyang, C.; Shi, S.; Lei, M. Ab Initio Studies on Atomic and Electronic Structures of Black Phosphorus. *J. Appl. Phys.* **2010**, *107*, 093178.

(36) Wang, X.; Sun, G.; Li, N.; Chen, P. Quantum Dots Derived from Two-Dimensional Materials and Their Applications for Catalysis and Energy. *Chem. Soc. Rev.* **2016**, *45*, 2239–2262.

(37) Zhou, Q.; Chen, Q.; Tong, Y.; Wang, J. Light-Induced Ambient Degradation of Few-Layer Black Phosphorus: Mechanism and Protection. *Angew. Chemie - Int. Ed.* **2016**, *55*, 11437–11441.

(38) Lin, S.; Chui, Y.; Li, Y.; Lau, S. P. Liquid-Phase Exfoliation of Black Phosphorus and Its Applications. *FlatChem* **2017**, *2*, 15–37.

(39) Sun, Z.; Xie, H.; Tang, S.; Yu, X. F.; Guo, Z.; Shao, J.; Zhang, H.; Huang, H.; Wang, H.; Chu, P. K. Ultrasmall Black Phosphorus Quantum Dots: Synthesis and Use as Photothermal Agents. *Angew. Chemie - Int. Ed.* **2015**, *54*, 11526–11530.

(40) Woomer, A. H.; Farnsworth, T. W.; Hu, J.; Wells, R. A.; Donley, C. L.; Warren, S. C. Phosphorene: Synthesis, Scale-Up, and Quantitative Optical Spectroscopy. *ACS Nano* **2015**, *9*, 8869–8884.

(41) Zhu, C.; Xu, F.; Zhang, L.; Li, M.; Chen, J.; Xu, S.; Huang, G.; Chen, W.; Sun, L. Ultrafast Preparation of Black Phosphorus Quantum Dots for Efficient Humidity Sensing. *Chem. - A Eur. J.* **2016**, *22*, 7357–7362.

(42) Zhu, X.; Zhang, T.; Sun, Z.; Chen, H.; Guan, J.; Chen, X.; Ji, H.; Du, P.; Yang, S. Black Phosphorus Revisited: A Missing Metal-Free Elemental Photocatalyst for Visible Light Hydrogen Evolution. *Adv. Mater.* **2017**, *29*.

(43) Wang, H.; Yang, X.; Shao, W.; Chen, S.; Xie, J.; Zhang, X.; Wang, J.; Xie, Y. Ultrathin Black Phosphorus Nanosheets for Efficient Singlet Oxygen Generation. *J. Am. Chem. Soc.* **2015**, *137*, 11376–11382.

(44) Wang, X.; Maeda, K.; Thomas, A.; Takanabe, K.; Xin, G.; Carlsson, J. M.; Domen, K.; Antonietti, M. A Metal-Free Polymeric Photocatalyst for Hydrogen Production from Water under Visible Light. *Nat. Mater.* **2009**, *8*, 76–80.

(45) Tian, B.; Tian, B.; Smith, B.; Scott, M. C.; Hua, R.; Lei, Q.; Tian, Y. Supported Black Phosphorus Nanosheets as Hydrogen-Evolving Photocatalyst Achieving 5.4% Energy Conversion Efficiency at 353 K. *Nat. Commun.* **2018**, *9*, 1–11.

(46) Nocera, D. G. The Artificial Leaf. *Acc. Chem. Res.* **2012**, *45*, 767–776.

(47) Muduli, S. K.; Varrla, E.; Xu, Y.; Kulkarni, S. A.; Katre, A.; Chakraborty, S.; Chen, S.; Sum, T. C.; Xu, R.; Mathews, N. Evolution of Hydrogen by Few-Layered Black Phosphorus under Visible Illumination. *J. Mater. Chem. A* **2017**, *5*, 24874–24879.

(48) Ni, M.; Leung, M. K. H.; Leung, D. Y. C.; Sumathy, K. A Review and Recent Developments in Photocatalytic Water-Splitting Using TiO_2 for Hydrogen Production. *Renew. Sustain. Energy Rev.* **2007**, *11*, 401–425.

(49) Panigrahi, S.; Kundu, S.; Ghosh, S. K.; Nath, S.; Pal, T. General Method of Synthesis for Metal Nanoparticles. *J. Nanoparticle Res.* **2004**, *6*, 411–414.

(50) Islam, A.; Anwarul Kabir Bhuiya, M.; Saidul Islam, M. A Review on Chemical Synthesis Process of Platinum Nanoparticles. *Asia Pacific J. Energy Environ.* **2014**, *1*, 107.

(51) Kang, J.; Wood, J. D.; Wells, S. A.; Lee, J. H.; Liu, X.; Chen, K. S.; Hersam, M. C. Solvent Exfoliation of Electronic-Grade, Two-Dimensional Black Phosphorus. *ACS Nano* **2015**, *9*, 3596–3604.

(52) Daasch, L. W.; Smith, D. C. Infrared Spectra of Phosphorus Compounds. *Anal. Chem.* **1951**, *23*, 853–868.

(53) Kamat, P. V. Quantum Dot Solar Cells. Semiconductor Nanocrystals as Light Harvesters. *J. Phys. Chem. C* **2008**, *112*, 18737–18753.

(54) Hanlon, D.; Backes, C.; Doherty, E.; Cucinotta, C. S.; Berner, N. C.; Boland, C.; Lee, K.; Harvey, A.; Lynch, P.; Gholamvand, Z., Liquid Exfoliation of Solvent-Stabilized Few-Layer Black Phosphorus for Applications beyond Electronics. *Nat. Commun.* **2015**, *6*, 1–11.

(55) Ebbesen, T. W.; Ferraudi, G. Photochemistry of Methyl Viologen in Aqueous and Methanolic Solutions. *J. Phys. Chem.* **1983**, *87*, 3717–3721.

(56) Prasad, D. R.; Hoffman, M. Z. Charge-Transfer Complexation between Methylviologen and Sacrificial Electron Donors EDTA, Triethanolamine, and Cysteine. *J. Phys. Chem.* **1984**, *88*, 5660–5665.

(57) Zou, X.; Zhang, Y. Noble Metal-Free Hydrogen Evolution Catalysts for Water Splitting. *Chem. Soc. Rev.* **2015**, *44*, 5148–5180.

(58) Wu, G. W.; He, S. Bin; Peng, H. P.; Deng, H. H.; Liu, A. L.; Lin, X. H.; Xia, X. H.; Chen, W. Citrate-Capped Platinum Nanoparticle as a Smart Probe for Ultrasensitive Mercury Sensing. *Anal. Chem.* **2014**, *86*, 10955–10960.